NIST Measurement Services:

Natural Gas Flow Calibration Service (NGFCS)

NIST Special Publication 1081

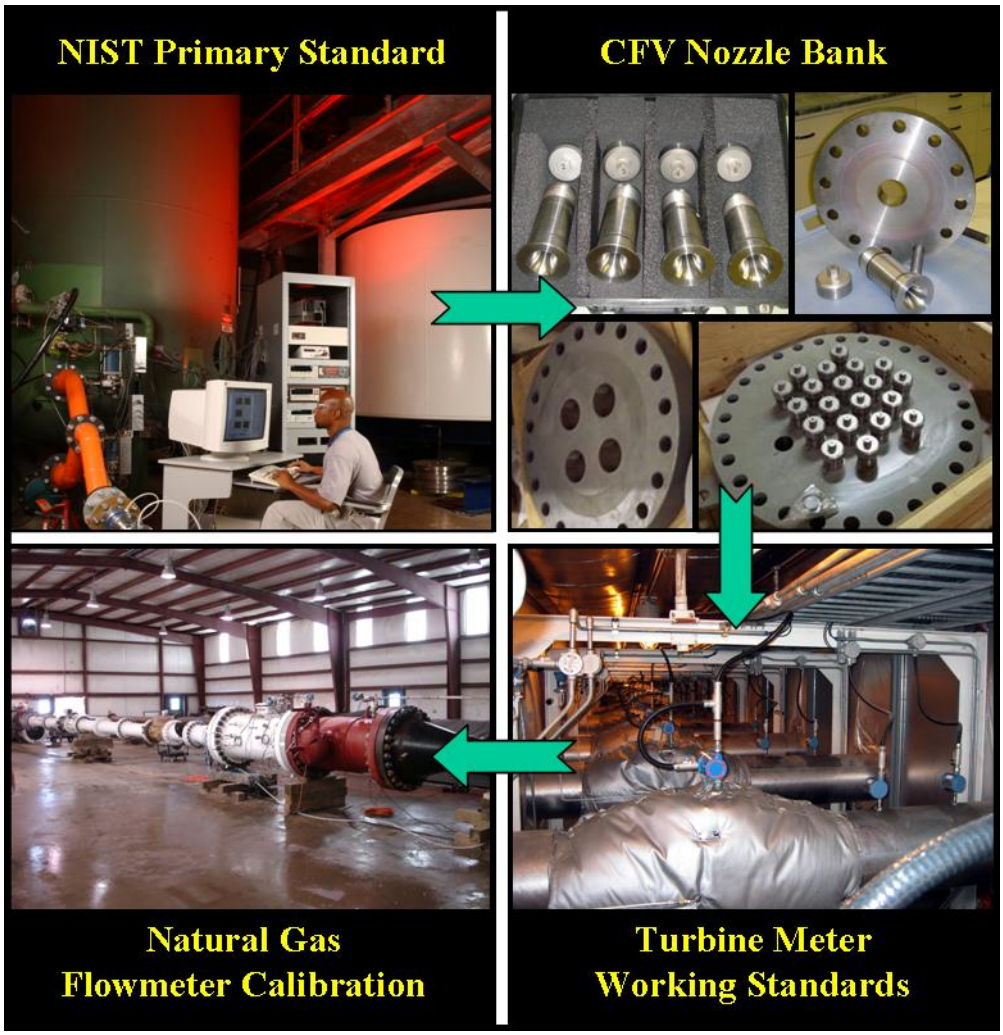

Aaron N. Johnson

U. S. Department of Commerce
Technology Administration
National Institute of Standards and Technology

Table of Contents for the Natural Gas Flowmeter Calibration Service (NGFCS)

Abstract

This document describes NIST's high pressure natural gas flow calibration service (NGFCS). Flow calibrations are conducted offsite at the Colorado Experimental Engineering Station Incorporated (CEESI) in Garner, Iowa. A parallel array of nine turbine meter working standards (TMWS) are used to calibrate customer flowmeters over a flow range from 0.25 m^3/s to 9 m^3/s at nominal pressures of 7500 kPa and at ambient temperatures. Over this flow range the expanded uncertainty varies from 0.25 % to 0.27 % (increasing at lower flows). All flowmeter calibrations are traceable to NIST standards. In particular, each of the nine TMWS is traceable to the NIST's primary flow standards via a bootstrap process using critical flow venturis (CFVs), while auxiliary measurements (*e.g.*, pressure, temperature, frequency, etc.) are traceable to the appropriate NIST standard. This document provides a detailed analysis of the bootstrap procedure used to establish NIST traceability and the uncertainty of this procedure. In addition, the document gives information about the flow measurement capabilities of the NGFCS (*i.e.*, types of meters calibrated, calibration setup, calibration procedures, a sample calibration report, etc.).

1. INTRODUCTION

NIST has extended its flow measurement capabilities to include natural gas flows at pressures and temperature conditions commensurate with U.S. gas pipeline distribution companies. Because NIST does not have natural gas flow measurement facilities of the necessary scale, a new approach has been developed that utilizes Cooperative Research and Development Agreements (CRADA) and Qualified Manufacturers Listings (QML) to augment NIST primary flow measurement standards. This combination is the basis for a new NIST flowmeter calibration service for large flowmeters ranging in size from 200 mm to 750 mm (8 inches to 30 inches) diameter that operate over a pressure range of approximately 6.2 MPa to 9 MPa (900 psi to 1 300 psi) at ambient temperature in natural gas flows. To realize these capabilities NIST has established a QML for private sector suppliers having the capability of providing the necessary facilities and operational expertise. Currently one provider, Colorado Engineering Experiment Station, Inc. (CEESI), has met this NIST QML requirement. To establish and improve the necessary chain of traceability to the SI, NIST engages in collaborative research efforts with CEESI under the terms of a Cooperative Research and Development Agreement (CRADA) These efforts ensure that improvements in NIST primary flow measurement standards, in working standards used in establishing traceability, and in improvements to metrological control capabilities are implemented in a timely and efficient manner.

NIST works with CEESI in two distinct modes to provide this calibration service. In the operational mode, NIST uses the QML to purchase services provided by CEESI for individual calibration tests for a particular NIST customer. The test data obtained is derived from procedures and protocols specified by NIST that are performed at CEESI under NIST metrological control. CEESI provides access to its facilities and the expertise necessary to test the metering device of a customer at an agreed upon cost. Under the terms of the CRADA NIST and CEESI engage in cooperative research efforts to develop and improve the traceability ladder that extends NIST's on-site, primary, gas flowrate measurement standards to the pipeline conditions attained at CEESI's Garner, Iowa test site. These research efforts investigate flow phenomena affecting the traceability ladder with the intent of improving various aspects of flow traceability. The result of these joint activities is the Natural Gas Flow Calibration Service (NGFCS).

A key aspect of the NGFCS is that NIST maintains metrological control of flowmeter calibrations performed at CEESI's Garner, Iowa facility. The following measures are taken by NIST to ensure metrological control:

1) A path of traceability is established and maintained linking the calibration of a meter under test (MUT) at CEESI to NIST's primary flow standards.
2) The NIST quality system, compliant with ISO 17025 [i], is extended to these calibration activities.
3) Each calibration is monitored via a secure internet connection.
4) All auxiliary instrumentation (*e.g.*, pressure transducers, temperature sensors, frequency counters, etc.) necessary for flow calibrations are traceable to NIST via transfer standards provided by and maintained by NIST.
5) Control charts that validate the performance of both auxiliary instrumentation and flowmeter check standards are maintained by NIST.
6) The calibration process is highly automated to increase reproducibility and decrease the risk of human error.

7) Diagnostics are used to quantify flow stability levels, line pack (or mass storage) effects, the impact of changing environmental conditions, and other parameters affecting calibration results.
8) The results of each flowmeter calibration are validated by a check standard installed in series with the meter under tests (MUT).
9) The raw calibration data is analyzed by NIST.
10) The calibration report is written by NIST.
11) The facility is periodically compared to other national metrology institutes within the framework of the CIPM Mutual Recognition Arrangement (*i.e.*, international key comparisons) to detect potential biases in the calibration results.

The focus of this document is to provide a description of the traceability ladder that extends from NIST's primary flow standards to the working standards used for flow meter calibration at pipeline conditions. It is also a reference guide for customers looking for specific information about operational aspects of NIST's natural gas flow calibration service (*e.g.*, types and sizes of flowmeters that can be calibrated, flow capacity, how to schedule a calibration, cost of a calibration, turnaround time, etc.) as well as a technical resource that provides the underlying metrological details of how flow traceability to NIST is established and the uncertainty budget resulting from this process.

2. DESCRIPTION OF MEASURMENT SERVICES

NIST calibration services are continuously being upgraded. Customers should consult the following web address http://www.cstl.nist.gov/div836/Group_02/index_836.02.html to find the most current information regarding the calibration services (*e.g.*, calibration fees, turnaround times, technical contacts, shipping procedures, etc.).

Table 2.1. Typical natural gas concentration at CEESI's Iowa flow facility.

Component	Mole (%)
Methane	94.8 to 96.2
Ethane	1.5 to 2.3
Propane	0.055 to 0.3
iButane	0.0008 to 0.03
nButane	0.0003 to 0.04
iPentane	0 to 0.01
nPentane	0 to 0.006
C6+	0 to 0.006
Nitrogen	1.4 to 1.8
Carbon Dioxide	0.5 to 0.7
Hydrogen	0.05 to 0.27
Helium	0.03 to 0.04

2.1 Flow Capacity and Capabilities of the NGFCS

The NGFCS can calibrate both volumetric based and mass based flowmeters. The volumetric flow range extends from 0.25 m^3/s (1.5×10^4 L/min or 3.2×10^4 acfh) to 9 m^3/s (5.4×10^5 L/min or 1.14×10^6 acfh) at a nominal pipeline pressure of 7 500 kPa ± 1 200 kPa (1 088 psi ± 174 psi) and at a nominal temperature of 292.5 K ± 7.5 K (66.8 °F ± 13.5 °F). [1] The expanded uncertainties for volumetric flow calibrations vary from 0.25 % to 0.27 %, increasing at lower flows. Mass flow capabilities extend from 5.9 kg/s (13.1 lbm/s) to 533 kg/s (1175.8 lbm/s) with uncertainties ranging from 0.26 % to 0.28 % depending on flow. The typical natural gas composition for flow calibrations is shown in Table 2.1.

NIST is working toward extending the calibration flow range to 0.1 m^3/s and to reducing the uncertainty to 0.2 % over the entire flow range. The following website http://www.cstl.nist.gov/div836/Group_02/index_836.02.html should be consulted for current capabilities.

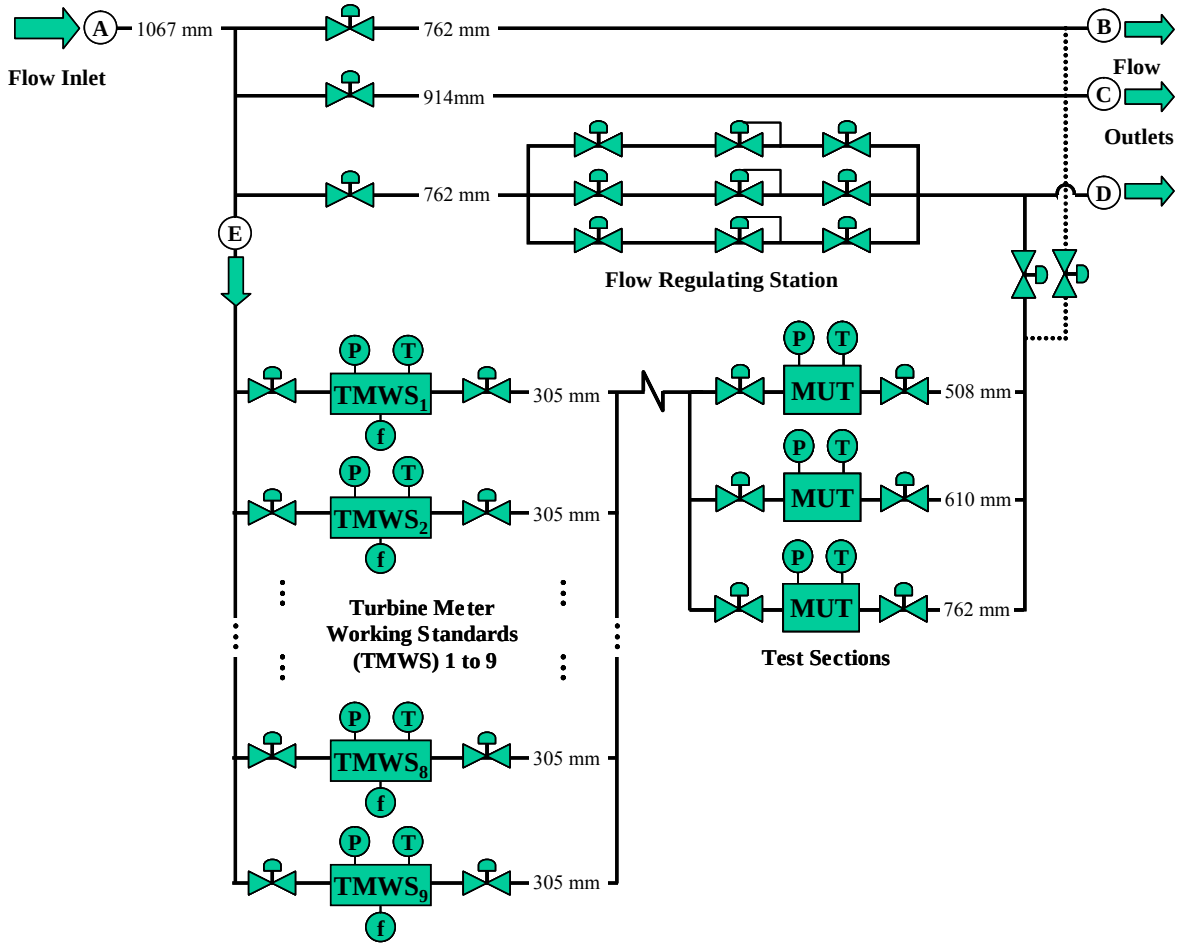

Figure 2.1. CEESI Iowa Flowmetering Facility

[1] Note that the variation in pressure and temperature occur seasonally, and not during a flowmeter calibration.

2.2 Description of the Calibration Facility

NIST flow calibrations are conducted at CEESI's Iowa flow facility. This facility is shown in Fig. 2.1. The dry pipeline quality natural gas that enters the custody transfer junction in pipeline A is transported throughout the northwest region of the United States in pipelines B, C, and D.

During a flowmeter calibration a fraction of the gas from pipeline A is diverted to pipeline E where it is measured by a parallel array of up to nine turbine meter working standards (TMWS). The flow measured by the TMWS is used to determine the flow at the MUT installed downstream in one of three appropriately sized test sections. Flow exiting the MUT is returned to pipelines B, C, and/or D as appropriate.

A gas chromatograph (not shown in the figure) located upstream of the TMWS array on pipeline E is used to measure the gas composition. Each of the nine TMWS is instrumented with a pair of pressure transducers, a pair of temperature sensors, and a pair of frequency counters. The redundant measurements guard against erroneous instrumentation readings. The MUT is also instrumented with redundant pressure and temperature instrumentation (and frequency when necessary).

2.3 Mathematical Formulation of Volumetric and Mass Flow

Application of the principle of conservation mass shows that the mass flow at the MUT equals

$$\dot{m}_{\mathrm{MUT}} = \sum_{\mathrm{n}=1}^{9} \dot{m}_{\mathrm{TMWS,n}} \delta_{\mathrm{n}} - \Delta\dot{m}_{\mathrm{st}} - \dot{m}_{\mathrm{leak}} \tag{2.1}$$

where $\dot{m}_{\mathrm{TMWS,n}}$ is the mass flow through the n$^{\mathrm{th}}$ TMWS; δ_{n} is the TMWS selector function, which equals zero when the n$^{\mathrm{th}}$ TMWS shutoff valve is closed (*i.e.*, no flow) and unity when it is open; $\Delta\dot{m}_{\mathrm{st}}$ is the rate of mass storage (or line pack) in the connecting pipe volume between the TMWS and the MUT; and $\dot{m}_{\mathrm{leak}}$ is the net rate of mass leakage out of the connecting volume. Leak check procedures ensure that $\dot{m}_{\mathrm{leak}}$ is negligible relative to the measured flow. Similarly, stable flow conditions are maintained so that $\Delta\dot{m}_{\mathrm{st}}$ is small relative to $\dot{m}_{\mathrm{MUT}}$. Consequently, both $\dot{m}_{\mathrm{leak}}$ and $\Delta\dot{m}_{\mathrm{st}}$ are taken to be zero when computing $\dot{m}_{\mathrm{MUT}}$, but are included in the uncertainty budget. With this simplification the mass flow at the MUT is

$$\dot{m}_{\mathrm{MUT}} = \sum_{\mathrm{n}=1}^{N} \rho_{\mathrm{TMWS,n}} q_{\mathrm{TMWS,n}} \delta_{\mathrm{n}} \,. \tag{2.2}$$

where the product of density ($\rho_{\mathrm{TMWS,n}}$) and volumetric flow ($q_{\mathrm{TMWS,n}}$) is substituted for mass flow.

The volumetric flow measured by the n$^{\mathrm{th}}$ TMWS is proportional to the rotational frequency of the respective turbine blade ($f_{\mathrm{TMWS,n}}$)

$$q_{\mathrm{TMWS,n}} = \frac{f_{\mathrm{TMWS,n}}}{K_{\mathrm{TMWS,n}}} \tag{2.3}$$

where the inverse of the meter factor or *K*-factor ($K_{\mathrm{TMWS,n}}$) is the constant of proportionality. The *K*-factor of each TMWS is traceable to NIST primary flow standards via an array of critical flow venturis (CFVs). The measurement results and uncertainties of this traceability chain are outlined in Section 3 and discussed in detail in Section 4. Substitution of Eqn. 2.3 into Eqn. 2.2 yields an expression for mass flow entirely in terms of parameters associated with the turbine meter

$$\dot{m}_{\mathrm{MUT}} = \sum_{\mathrm{n}=1}^{N} \delta_{\mathrm{n}} \rho_{\mathrm{TMWS,n}} \left(\frac{f_{\mathrm{TMWS,n}}}{K_{\mathrm{TMWS,n}}} \right). \tag{2.4}$$

The expression for volumetric flow is derived by dividing by the density at the MUT (ρ_{MUT})

$$q_{\mathrm{MUT}} = \sum_{\mathrm{n}=1}^{N} \left(\frac{\rho_{\mathrm{TMWS,n}}}{\rho_{\mathrm{MUT}}} \right) \left(\frac{f_{\mathrm{TMWS,n}}}{K_{\mathrm{TMWS,n}}} \right) \delta_{\mathrm{n}} . \tag{2.5}$$

Alternative formulations for mass flow (Eqn. 2.4) and for volumetric flow (Eqn. 2.5) can be derived by using the equation of state for gas density

$$\rho = \frac{P\mathcal{M}}{Z R_{\mathrm{u}} T} \tag{2.6}$$

where P and T are respectively, the measured pressure and temperature, R_{u} is the universal gas constant, Z is the compressibility factor as determined from REFPROP 8 Thermodynamic Database [ii], and $\mathcal{M}_{\mathrm{NG}} = \sum M_{\mathrm{k}} x_{\mathrm{k}}$ is the molar mass of the natural gas mixture - a linear sum of M_{k} (the molar mass of the k$^{\mathrm{th}}$ component) multiplied by x_{k} (the mole fraction of the k$^{\mathrm{th}}$ component) summed over all the mixture components. Combining Eqn. 2.6 with Eqns. 2.4 and 2.5 respectively yields the following formulation for mass flow

$$\dot{m}_{\mathrm{MUT}} = \sum_{n=1}^{N} \delta_{\mathrm{n}} \left[\frac{P_{\mathrm{n}} \mathcal{M}_{\mathrm{NG}} f_{\mathrm{n}}}{Z_{\mathrm{n}} R_{\mathrm{u}} T_{\mathrm{n}} K_{\mathrm{n}}} \right]_{\mathrm{TMWS}} \tag{2.7}$$

and volumetric flow

$$q_{\mathrm{MUT}} = \sum_{n=1}^{N} \delta_{\mathrm{n}} \left(\frac{P_{\mathrm{TMWS,n}}}{P_{\mathrm{MUT}}} \right) \left(\frac{T_{\mathrm{MUT}}}{T_{\mathrm{TMWS,n}}} \right) \left(\frac{Z_{\mathrm{MUT}}}{Z_{\mathrm{TMWS,n}}} \right) \left(\frac{f_{\mathrm{TMWS,n}}}{K_{\mathrm{TMWS,n}}} \right), \tag{2.8}$$

respectively.

2.4 General Calibration Procedures

The general procedures for calibrating a MUT are divided into four parts including A) installation procedures, B) pre-flow calibration checks and procedures, C) flow calibration procedures, and D) post processing calibration procedures. Here, we summarize these procedures for a typical calibration. The full lists of procedures are included in the NIST NGFCS Quality Manual.

A. Installation Procedures

1. Install MUT in the appropriately sized test section:
   a. *Upstream and downstream piping will be a minimum of 10 D and 5 D respectively unless otherwise specified where D is the pipe diameter.*
   b. *Check to ensure that inside diameter of the upstream piping is within 1 % of the meter bore or the manufacturer's specifications. Make sure that there is not a observable discontinuity in diameter between upstream diameter and meter bore diameter.*
   c. *Ensure flange faces at the inlet and exit of the meter match up with inlet and exit piping.*
   d. *Upstream flanges and gaskets shall not protrude into the flow stream by more than 1 % of the internal pipe diameter.*
2. Install thermal well(s)/temperature transmitter(s) between 1 *D* and 5 *D* downstream of the meter.
3. Install pressure transmitters.
4. Document (sketch), upstream and downstream piping, the location of pressure and temperature taps, and other fittings relative to MUT.
5. Photograph calibration setup including MUT and instrumentation.

B. Pre-Flow Calibration Checks and Procedures

1. Remove any air left in the pipeline from meter installation.
2. Perform leak checks at 2 MPa, 4 MPa, 6 MPa, and at operating line pressures
3. Check proper operation of data acquisition system including readouts of pressure, temperature, and frequency.

Table 2.2. Sequence of flow set points for a typical calibration. (Second half of dataset is used to assess hysteresis effects and reproducibility)

Set Point Number	Flow Set Point	No. of Repeats at Set Point
1	q_{min} (Typically 55 m/min or 3 ft/s)	3
2	10 % of q_{max}	3
3	25 % of q_{max}	3
4	40 % of q_{max}	3
5	70 % of q_{max}	3
6	100 % of q_{max}	3
Interrupt and reestablish nominal flow		
7	100 % of q_{max}	3
8	70 % of q_{max}	3
9	40 % of q_{max}	3
10	25 % of q_{max}	3
11	10 % of q_{max}	3
12	q_{min} (Typically 55 m/min or 3 ft/s)	3
13	1 Verification Point taken (between 40 % and 70 % of q_{max})	1

C. Calibration Procedures

1. Determine the minimum ($q_{\min}$) and maximum ($q_{\max}$) flows for the calibration.
2. Determine the appropriate flow set points (see Table 2.2).
3. Determine how many of the nine TMWS are needed to achieve the flow set points.
4. Establish steady flow through the MUT at the desired flow set points.
5. Data Collection and Calculations:
   a. *Collect data (i.e., temperature, pressure, and frequency necessary for flow determination) for approximately 120* s. *(The software data rate is about 1* Hz *so that approximately 120 points are collected).*
   b. *The software calculates the desired flow at all 120 points using Eqn. 2.7 for mass flow or Eqn. 2.8 for volumetric flow.*
   c. *The time averaged value of volumetric flow (or mass flow) is defined as the arithmetic average of the 120 flow points.*
   d. *The flow set point is repeated as specified in Table 2.2.*
6. Follow the protocol in Table 2.2.
   a. *If the current set point number is not equal to either 6 or 12 then increment the set point number by one and return to step 2.*
   b. *If the current set point number equals 6 then interrupt and reestablish the nominal flow before returning to step 2 and starting set point number 7.*
   c. *If set point number 12 has just been completed proceed to step 7.*
7. If an ultrasonic flowmeter is being calibrated, then calculate the Flow Weighted Mean Error (FWME) per AGA 9 [iii].
   a. *Electronically install the FWME adjustment into the ultrasonic flowmeter.*
   b. *If directed by customer and suitable for the meter design multi-point linearization techniques will be used to electronically install adjustment.*
   b. *Once the meter factor(s) is electronically installed, 1 verification point shall be taken as denoted in Table 2.2 (Note that verification points are performed only if electronic adjustments are made to the flowmeters).*
   c. *Upon completion of the Verification point, if available, the meter shall be put into a "Read Only" mode.*

D. Post Processing Calibration Procedures

1. Raw data sent to NIST electronically.
2. NIST checks stability criteria to assess the quality of the data.
3. NIST ensures data is consistent with check standards used in series with the MUT during the calibration.
4. If data quality is acceptable, NIST processes data and compares results to values determined by the software at the time of calibration.
5. NIST checks to ensure post processed calibration factors match those electronically installed in ultrasonic flowmeter.
6. NIST writes and sends out the calibration report.

2.5 Available Pipeline Sizes and Required Safety Inspection for Flanges

Flowmeters can be calibrated in pipe sizes ranging from 30.48 cm (12 inches) to 76.2 cm (30 inches). When a customer submits upstream and downstream pipe lengths along with the flowmeter to be calibrated, the associated flanges should be rated to withstand a minimum pressure of 10 MPa at ambient temperatures (*i.e.*, flange ratings must be 600 lb or higher).

Additionally, for safety reasons, customers must have all flange welds x-rayed and hydrostatically tested before shipping their flowmeters for calibration.

2.6 Flowmeter Types Typically Calibrated

The vast majority of flowmeters calibrated by the NGFCS are ultrasonic flowmeters that are used for the custody transfer of natural gas. However, other flowmeters types can also be calibrated. Table 2.3 shows a list of flowmeters types that are calibrated. Some flowmeter types not listed here may also be suitable for calibration. Contact NIST staff for details.

Table 2.3 Typical Flowmeters Calibrated

Flowmeter Types
Ultrasonic Flowmeters
Turbine Flowmeters
V-Cone Flowmeters
Coriolis Meters
Subsonic Venturis/Nozzles
Sonic Venturis/Nozzles
Positive Displacement Meters
Variable Area Flowmeters (Rotameters)
Vortex Shedding Flowmeters

2.7 Procedures for Submitting a Flowmeter for Calibration

The Fluid Metrology Group follows the policies and procedures described in Chapters 1, 2, and 3 of the NIST Calibration Services Users Guide [iv]. These chapters can be found on the internet at the following addresses:

1. http://ts.nist.gov/ts/htdocs/230/233/calibrations/Policies/policy.htm
2. http://ts.nist.gov/ts/htdocs/230/233/calibrations/Policies/domestic.htm
3. http://ts.nist.gov/ts/htdocs/230/233/calibrations/Policies/foreign.htm

Chapter 2 gives instructions for ordering a calibration for domestic customers and has the sub-headings: (A) Customer Inquiries; (B) Pre-arrangements and Scheduling; (C) Purchase Orders; (D) shipping, Insurance, and Risk of Loss; (E) Turnaround Time; and (F) Customer Checklist. Chapter 3 gives special instructions for foreign customers.

3. OVERVIEW OF THE PROCESS USED TO ESTABLISH TRACEABILITY

This section gives an overview of the five stage procedure used to establish the traceability chain between a flowmeter calibrated at CEESI's Iowa facility back to NIST's primary flow standards. A key element of the five stage process was the critical flow venturi (CFV) bootstrap process. NIST's low pressure, low flow standards were used to calibrate multiple CFVs, which were used in parallel to provide traceability at pipeline conditions for natural gas flows. A description of the CFVs and their basic calibration parameters are described, and an overview of the uncertainty attributed to this scale-up procedure is presented.

3.1 Overview of the Five Stage Procedure used to Establish NIST Traceability

The traceability chain linking flowmeters calibrated at CEESI's Iowa facility in natural gas to NIST's low pressure, air flow primary standard were accomplished in five stages. A diagram of the five stage process is shown in Fig. 3.1. The first column in each row identifies the calibration stage, followed by the flow standard, the reference flowmeter being calibrated, the fluid medium, the expanded uncertainty (*i.e.*, $k = 2$) of the reference flowmeter, and the calibrated flow (or Reynolds number) range of the reference flowmeter. The nominal pressure conditions for all five stages are also specified in the figure.

Stage	Standard	Reference Meter	Working Fluid	Expanded Uncertainty of Reference Flowmeter	Flow or Reynolds Number Range
1	**NIST 26 m³ *PVTt*** **NIST *PVTt***	**LP CFVs** **4 x** $P_0 \approx 350$ to 700 kPa	**Filtered dry air**	**0.10 %**	LP CFV *Re* Range **1.1×10^6** **to** **2.4×10^6**
2	**LP Nozzle Bank** $P_0 \approx 350$ to 700 kPa	**MP CFVs** (Upstream of LP CFVs) **4 x** 4x P_0	**Filtered dry air**	**0.13 %**	MP CFV *Re* Range **3.7×10^6** **to** **8.6×10^6**
3	**MP Nozzle Bank** 4x P_0	**HP CFVs** (Upstream of MP CFVs) **8 x** 16x P_0	**Filtered dry air**	**0.17 %**	HP CFV *Re* Range (dry air) **20×10^6** **to** **27.5×10^6**
4	**HP Nozzle Bank** $P_0 \approx 7500$ kPa	**TMWS** (Upstream of HP CFVs) **9 x** $P \approx 7500$ kPa	**Natural Gas**	**0.24 % to 0.25 %**	HP CFV *Re* Range (natural gas) **24×10^6** **to** **27.5×10^6**
5	**TMWS Array** **9 x** $P \approx 7500$ kPa	**MUT** (Downstream of TMS) MUT $P \approx 7500$ kPa	**Natural Gas**	**0.25 % to 0.27 %**	TMWS Flow Range **0.25 m³/s** **to** **9.0 m³/s** ($P \approx 7500$ kPa and $T \approx$ ambient)

Figure 3.1. Schematic of the five stage process used to establish traceability of a MUT at CEESI's Iowa natural gas flow facility to NIST 26 m³ *PVTt* primary flow standard.

In Stage 1, the NIST 26 m³ *PVTt* flow standard [v-vii] was used to successively calibrate four CFVs in air over a pressure range extending from 350 kPa to 700 kPa. For these CFVs this pressure range corresponded to a Reynolds numbers range from 1.1×10^6 to 2.4×10^6. The four CFVs are referred to throughout this document as the low pressure (LP) CFVs. The expanded uncertainty of each of the LP CFVs was 0.10 % as verified in Section 4.1.

In Stage 2, the four LP CFVs were combined in parallel and positioned downstream of a single CFV. Under choked flow conditions, the stagnation pressure (P_0) of the upstream CFV equaled four times that of the four downstream LP CFVs. In this way the upstream CFV is calibrated at pressures and flows four times greater than any one of the downstream LP CFVs. This calibration process was done in dry air. We repeated this procedure four times so that a total of four CFVs were calibrated in Stage 2, which are herein referred to as the medium pressure (MP) CFVs. The Reynolds number range of each MP CFV extended from 4.7×10^6 to 8.4×10^6, and the expanded uncertainty of each MP CFVs was 0.13 %. The calibration results and uncertainty analysis are documented in Section 4.2.

Stage 3 is analogous to Stage 2. The four MP CFVs were combined in parallel and used to calibrate a single upstream CFV in dry air at four times the pressure. A total of eight CFVs were calibrated in Stage 3, which are herein referred to as high pressure (HP) CFVs. The boot-strapping approach implemented in Stages 2 and 3 resulted in eight HP CFVs that were traceable to the 26 m^3 *PVTt* primary standard, but with a flow capacity nearly sixteen times the Stage 1 calibration. The calibrated Reynolds number range of each HP CFV was 20×10^6 to 27.5×10^6 and the expanded uncertainty of each of the HP CFVs was 0.17 %. The calibration results and uncertainty analysis are documented in Section 4.3.

In Stage 4 the eight HP CFVs were combined in parallel and used to calibrate a total of nine TMWS, one at a time, *in natural gas*, *at the nominal pressures for which they are used, and mounted in the location of pipeline where they are used*. Reynolds number matching was used to apply the air-based calibration of the HP CFVs to natural gas. At these high Reynolds numbers (*i.e.*, above 16×10^6), theoretical predictions indicated a difference in the CFV discharge coefficient between dry air and natural gas of less than 0.01 % [viii]. Each of the TMWS was calibrated over a nominal volumetric flow range from 0.25 m^3/s (3.2×10^4 acfh) to 1 m^3/s (1.3×10^5 acfh) at nominal pipeline pressures of 7500 kPa and ambient temperatures. The volumetric flow was changed by varying the number of HP CFVs. The expanded uncertainty of each of the TMWS ranged from 0.24 % to 0.25 % depending on flow. The calibration results and uncertainty analysis are documented in Section 4.4.

In Stage 5, the nine TMWS are combined in a parallel array, and used to calibrate customer flowmeters (MUT) in natural gas at ambient temperatures and at nominal pipeline pressures of 7500 kPa. The flow range of the facility extends from a minimum of 0.25 m^3/s (3.2×10^4 acfh) when only a single TMWS is used to a maximum of 9 m^3/s (1.1×10^6 acfh) when all nine TMWS are used together at their full capacity. The expanded uncertainty of a MUT (not including the repeatability of the MUT) is 0.25 % at the highest flow and increases to 0.27 % at the lowest flow. The uncertainty analysis is documented in Section 4.5.

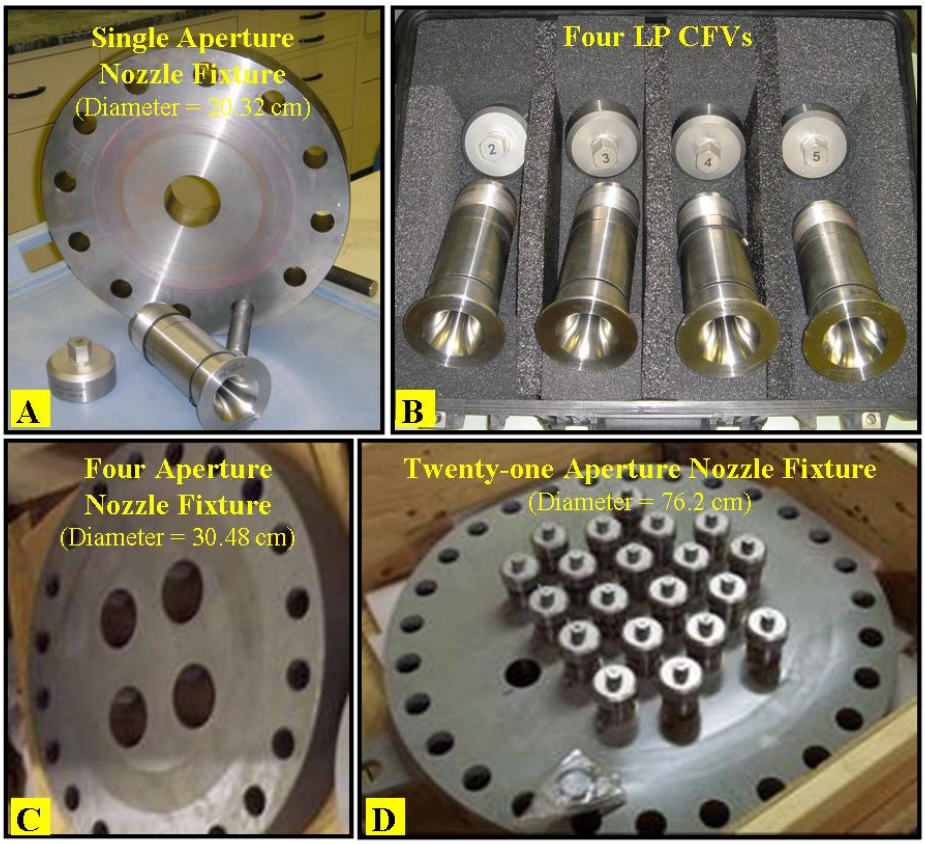

Figure 3.2 Four Photographs showing the CFVs with end caps and three different size nozzle fixtures

Figure 3.2 shows four photographs that include (A) the single aperture nozzle fixture used in Stage 1 to calibrate the LP CFVs; (B) the four LP CFVs with end caps (C) the four aperture nozzle fixture used both in Stage 2 to hold the four LP CFVs and again in Stage 3 to hold the four MP CFVs, and (D) the twenty-one aperture nozzle fixture used in Stage 4 to calibrate the nine TMWS. In Stage 4, the maximum flow was obtained with the HP CFVs mounted in only eight of the possible twenty-one apertures. Additional apertures (which allow for higher flows in the future) were not used. The unused apertures remain sealed for the entire calibration process. The end caps shown in Fig. 3.2 A, B, and D manually screw onto the downstream end of the CFVs to prevent flow. The end caps were used in the Stage 4 calibration of the TMWS using the eight HP CFVs. Initially, two of the eight HP CFVs were uncapped. The remaining six were systematically uncapped to change the volumetric flow through the TMWS being calibrated.

The apertures on the face of the nozzle fixtures in Fig. 3.2 A, C, and D, were dimensioned so that once the CFVs were installed they are both sealed and held in place by friction. When the nozzle fixture (with CFVs installed) was mounted in the pipeline, the pressure gradient necessary to choke the CFVs also added to the integrity of the seal. An illustration of the single CFV nozzle fixture installed in the appropriate sized pipeline is shown in Fig. 3.3. This figure corresponds to the Stage 1 calibration setup of the LP CFVs.

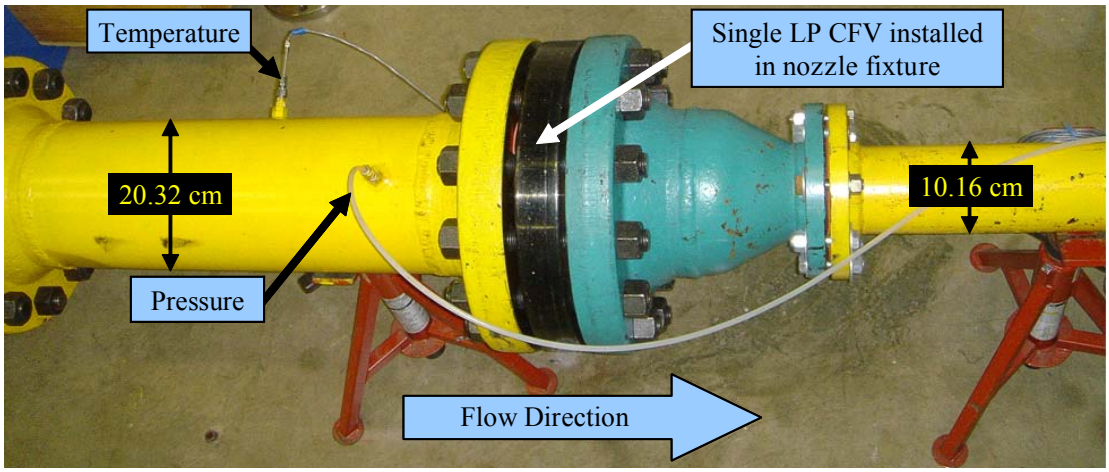

Figure 3.3. Stage 1 Calibration setup for LP CFVs

3.2 Description of CFVs and their Calibration Parameters

The LP, MP, and HP CFVs used to bootstrap between NIST low pressure, low air flow standard and pipeline scale flows of natural gas were designed according to the ISO 9300 standard [ix]. These flowmeters were selected because of their excellent reproducibility, simple geometric design, straightforward application, and well understood physics. The two dimensionless calibration parameters relevant for CFVs are the discharge coefficient (C_d) and the Reynolds number (Re). The discharge coefficient is a ratio of the actual mass flow ($\dot{m}$) to the theoretical mass flow ($\dot{m}_\mathrm{th}$) based on one-dimensional isentropic conditions. The theoretical mass flow is [x]

$$\dot{m}_\mathrm{th} = \frac{\pi d^2 P_0 C_s \sqrt{\mathcal{M}}}{4\sqrt{R_\mathrm{u} T_0}} \tag{3.1}$$

and the discharge coefficient is

$$C_\mathrm{d} \equiv \frac{\dot{m}}{\dot{m}_\mathrm{th}} = \frac{4\dot{m}\sqrt{R_\mathrm{u} T_0}}{\pi d^2 P_0 C_\mathrm{s} \sqrt{\mathcal{M}}} \tag{3.2}$$

where P_0 is the stagnation pressure, T_0 is the stagnation temperature, R_u is the universal gas constant, $\mathcal{M}$ is the molecular weight, d is the throat diameter, and C_s is the critical flow function. Appendix A explains how P_0, T_0, and C_s are calculated in this work. The Reynolds number definition used herein is

$$Re \equiv \frac{4\dot{m}_\mathrm{th}}{\pi \mu_0 d} = \frac{P_0 d C_\mathrm{s} \sqrt{\mathcal{M}}}{\mu_0 \sqrt{R_\mathrm{u} T_0}}, \tag{3.3}$$

where μ_0 is the dynamic viscosity evaluated at P_0, T_0. All thermodynamic properties are computed using the REFPROP 8.0 Thermodynamic Database [ii]. The calibration results for Stages 1 through 3 are expressed by plots of C_d versus Re.

Table 3.1 lists the throat diameters of the four LP CFVs (d_{LP}), the four MP CFVs (d_{MP}), and the eight HP CFVs (d_{HP}) referenced by their serial numbers. The throat diameters of the four LP CFVs were measured to tolerances better than 0.001 mm at a 95 % confidence level by the

Precision Engineering Division at NIST. The use of highly accurate d values cause the calibration data for the four LP CFVs to collapse onto a single curve that follows trends predicted by theoretical CFV models [xi-xiii]. The throat diameters of the MP and HP CFVs are defined so that the MP CFVs and the HP CFVs can be characterized by a single calibration curve that is consistent with the LP CFVs and with theory.

Table 3.1. LP CFVs measured d values and MP and HP CFVs estimated d values**.**

Total No. of CFVs	LP CFVs	d_{LP} (mm)	MP CFVs	d_{MP} (mm)	HP CFVs	d_{HP} (mm)
1	#2	25.3932	#10	25.3944	#1	25.4123
2	#3	25.3910	#11	25.3952	#7	25.3822
3	#4	25.3935	#12	25.3959	#8	25.3804
4	#5	25.3883	#13	25.3854	#14	25.3958
5	N/A	N/A	N/A	N/A	#15	25.3870
6	N/A	N/A	N/A	N/A	#17	25.3789
7	N/A	N/A	N/A	N/A	#19	25.3921
8	N/A	N/A	N/A	N/A	#20	25.4006

3.3 Summary of the Uncertainty of the Five Stage Calibration Process

The uncertainty of the five stage traceability scheme is determined using the GUM procedure [xiv]. The uncertainty for each of the five stages is summarized in the bar graph shown in Fig. 3.4. The height of each of the rectangles depicts the standard uncertainty (*i.e.*, $k = 1$) of the stage it represents. The sum of all five rectangles is 100 % and the root-sum-square of the standard uncertainties multiplied by a coverage factor of two is the expanded uncertainty (*i.e.*, $k = 2$) of the MUT. For flows ranging from 0.25 m^3/s to 9 m^3/s (at a nominal pressure of 7500 kPa and at ambient temperatures) the expanded uncertainty varies from 0.27 % to 0.25 %, decreasing with increasing flow.

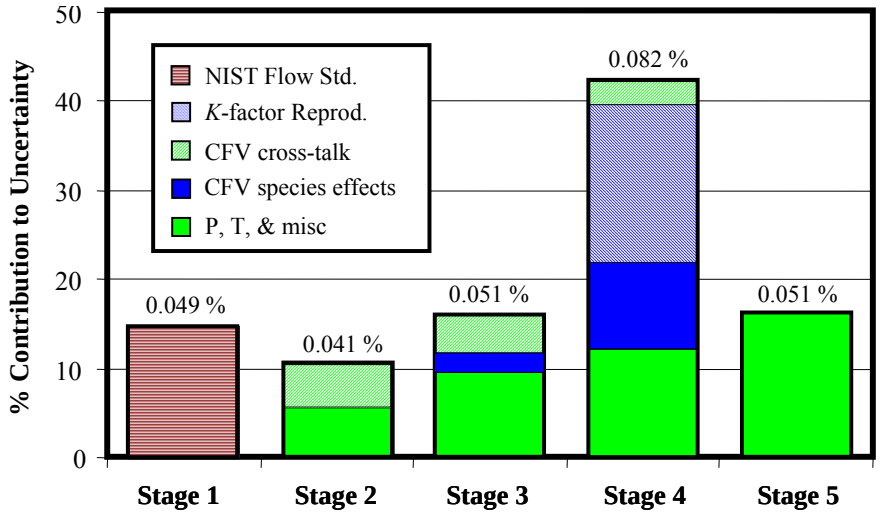

Figure 3.4. The standard uncertainty and the percent contribution to the total uncertainty of each stage for $q_{MUT} = 2.25$ m^3/s. (The height of each rectangle indicates the uncertainty contribution in percent for the corresponding stage.)

The legend in Fig. 3.4 shows the five different shading patterns used in the bar graph. The three lined shading patterns (*i.e.*, ▤, ▢, ▨) denote uncertainty components that NIST plans to reduce in the near future. These include the uncertainty introduced in Stage 1 corresponding to the NIST flow standard (▤), the uncertainty introduced in Stage 4 attributed to the reproducibility of the TMWS *K*-factors (▢), and the uncertainty introduced in Stages 2, 3, and 4 attributed to cross-talk (*i.e.*, interference effects) between the CFVs mounted in a common plenum (▨). The CFV interference effects will be reduced by increasing the spacing between the CFVs used in parallel. The *K*-factor reproducibility is currently based on only two calibrations. We anticipate lower values in the future as repeated calibrations provide a larger data set to more accurately determine the long term random effects and flowmeter drift. Lastly, NIST is currently working to reduce the uncertainty of the NIST flow standard used in Stage 1.

The two solid shading patterns (*i.e.*, ■ and ■) in Stages 2, 3, 4, and 5 include multiple uncertainty sources that have been grouped together. The first pattern of solid shading (■) includes uncertainty components attributed to pressure and temperature measurements, line pack effects, and various other sources. A detailed listing of the individual uncertainty components contained in these groupings is included in Section 4 and in references [xv, xvi].

The second pattern of solid shading (■) is attributed to CFV species effects. CFV species effects include uncertainty contributions from the following four thermodynamic properties: C_s for air in Stage 3, and C_s, Z, and $\mathcal{M}$ for natural gas in Stage 4. The cause of this uncertainty is twofold. First, the uncertainty attributed to C_s in Stages 3 and 4 is a consequence of calibrating the HP CFVs in air, but applying the calibration to natural gas. Second, the Stage 4 uncertainty attributed to Z and $\mathcal{M}$ results because the density of the natural gas is required to convert from the mass flow predicted by the HP CFVs to volumetric flow needed for the TMWS calibration. The uncertainties of these parameters are already nearly optimized, and are not likely to be reduced in the near future.

4. CALIBRATION ANALYSIS OF THE FIVE STAGE TRACEABILITY PROCESS

This section provides a detailed analysis of the calibration results and uncertainty for each of the five stages used to establish traceability to NIST. The governing calibration equations are developed for each of the five stages. The uncertainty introduced by each stage is determined using the method of propagation of uncertainty [xvii]. The GUM procedure [xviii] is followed whereby uncertainty sources are categorized as either Type A (*i.e.*, those which are evaluated by statistical methods) or Type B (*i.e.*, those which are evaluated by other means). Uncertainties having subcomponents belonging to both Type A and Type B are categorized as (A, B). The uncertainty analysis accounts for correlated uncertainty sources within and between each of the five stages.

In all five stages the flow properties (*e.g.*, the critical flow function, density, viscosity, etc.) are calculated using the REFPROP 8 Thermodynamic Database [ii]. In the first three stages the working fluid is air. The mole fraction of water vapor is maintained below 4.1×10^{-5} so that the air can be considered to be *dry air*. However, effects of water vapor are considered in the uncertainty budget. Table 4.1 shows the composition of dry air used to calculate flow properties in this work. The air composition is the average value of multiple references [xix- xxi].

Table 4.1 Composition of air used in Stages 1 through 3

Species	Mole Fraction (%)
Nitrogen	78.0849
Oxygen	20.9478
Argon	0.934
Carbon Dioxide	0.0314

4.1 STAGE 1: Calibration and Uncertainty of LP CFVs

Calibration of the LP CFVs

In Stage 1, NIST's 26 m^3 *PVTt* primary flow standard was used to calibrate the four LP CFVs in dry air. The *PVTt* flow standard uses a timed collection technique to determine the LP CFV mass flow. The flow emanating from the LP CFV was diverted from the bypass into the nearly evacuated collection tank for a measured time interval. The average gas temperature and pressure in the collection tank as well as in the inventory volume were measured before and after the filling process. These measurements were used in conjunction with the REFPROP 8 Thermodynamic Database [ii] to determine the initial and final densities of the gas in the collection tank (ρ_T^i and ρ_T^f), and in the inventory volume (ρ_I^i and ρ_I^f). In the absence of leaks, the time averaged mass flow equals the change in mass within the collection tank (*i.e.*, gas density change in the collection tank multiplied by the collection tank volume) plus the change in mass in the inventory volume (*i.e.*, gas density change in the inventory volume multiplied by the inventory tank volume) divided by the collection time

$$\dot{m} = \frac{(\rho_T^f - \rho_T^i)V_T + (\rho_I^f - \rho_I^i)V_I}{\Delta t} \tag{4.1}$$

where V_T is the collection tank volume; V_I is the inventory volume; and Δt is the collection time interval. The standard relative uncertainty of *PVTt* mass flow measurements is $[u(\dot{m})/\dot{m}] = 0.045$ %. A detailed description of the *PVTt* system and its uncertainty can be found in references [v-vii].

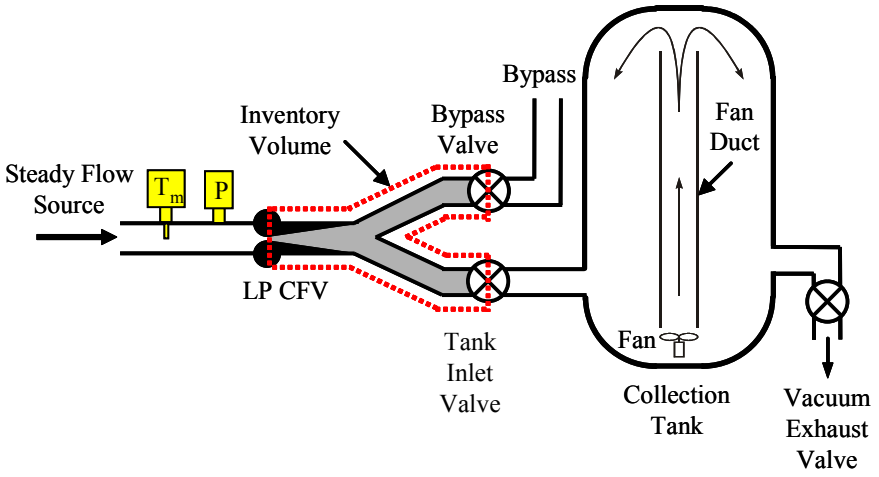

Figure 4.1. Schematic of NIST 26 m^3 *PVTt* Primary Flow Standard

The mass flows measured by the *PVTt* flow standard were used to calculate C_d values for each of the four LP CFVs using Eqn. 3.2, while the Reynolds number was computed using Eqn. 3.3. Figure 4.2 shows the calibration data for all four LP CFVs plotted on a logarithmic Reynolds number axis. Included in the figure are the results for the MP and HP CFVs. These results are plotted along with the LP CFV data so that general trends for all three stages of CFV calibration data (*i.e.*, Stages 1, 2, and 3) can be easily observed. The MP and HP CFV data, however, are not discussed in this section, but are covered in Sections 4.2 and Sections 4.3, respectively.

The LP CFV data shown in the figure incorporate two different *PVTt* calibrations, the first in 2004, and the second two years later in 2006. In both sets of calibration data the four LP CFVs are depicted by triangles having four different orientations. Open triangles are used for the 2004 dataset (*i.e.*, ◁ - CFV #2; ▽ - CFV #3; ▷ - CFV #4; △ - CFV #5) while closed triangles are used for the 2006 data set (*i.e.*, ◀ - CFV #2; ▼ - CFV #3; ◀ - CFV #4; ▲ - CFV #5). For clarity, this nomenclature is also denoted in the legend of Fig. 4.2. Each data point in the figure is the average of a minimum of four repeated *PVTt* flow measurements at the same nominal flow. In general, the standard deviation of the four (or more in some cases) repeated flow measurements is 0.006 %.

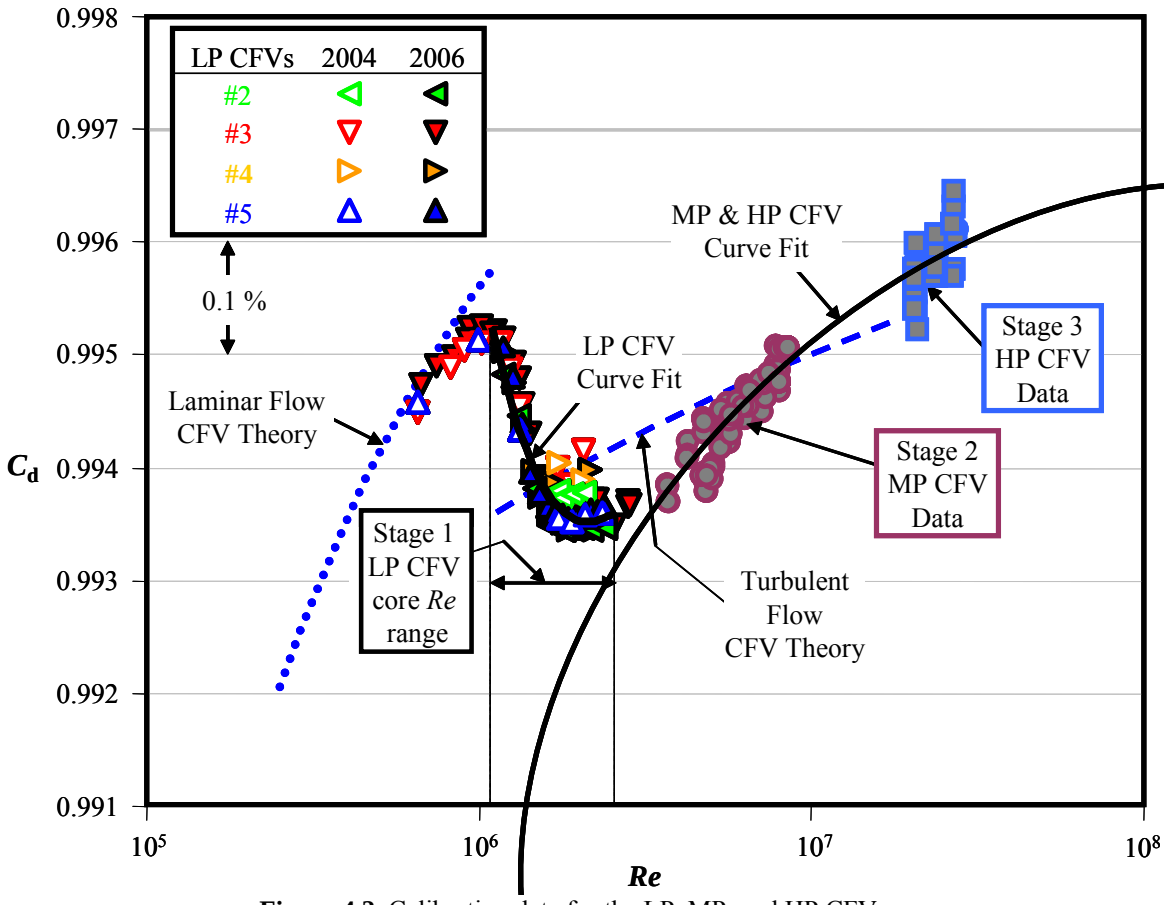

Figure 4.2. Calibration data for the LP, MP, and HP CFVs.

The theoretical C_d values for the laminar CFV flow model (·····) [viii] and the turbulent CFV flow model (- - - -) [viii] are plotted with the calibration data in Fig. 4.2 to clearly illustrate that

the LP CFV results lie almost entirely in the transitional flow regime. As expected, the portion of the calibration data below $Re < 10^6$ closely follows the laminar flow model. However, at higher Reynolds numbers the data falls slightly below the turbulent flow model. The apparent discrepancy at higher Reynolds numbers could be the result of the flow not being fully turbulent. In any circumstance the difference (*i.e.*, less than 0.1 %) is well within expected capability of the turbulent flow model.

In total, the LP CFV results include 95 data points that span a Reynolds number range from 6.5×10^5 to 2.8×10^6. However, only CFV #3 and CFV #5 were calibrated over this extended Reynolds number range. The core Reynolds number range for which all four LP CFVs were calibrated extends from 1.1×10^6 to 2.4×10^6, corresponding to stagnation pressures ranging from 350 kPa to 700 kPa at ambient temperatures. The data within the core Reynolds number range is used in Stage 2 when the array of LP CFVs are used to calibrate the MP CFVs. The Reynolds numbers values outside this core region were obtained primarily to ensure that the data followed the expected theoretical trends in the laminar and turbulent flow regimes. Within the core region, C_d values were measured at no less than 11 equally spaced Re to capture the changes in concavity that occur in the transitional flow regime. Considering that the core data includes four different LP CFVs, each calibrated twice two years apart, and that the data lies entirely in the transitional flow regime, the tight overlap between the data is remarkable. As indicated in the figure, the data in the core region for all four LP CFVs can be represented by a single calibration curve

$$C_{d,FIT}^{LP} = b_0 + b_1 Re^{-1/5} + b_2 Re^{-2/5} \tag{4.2}$$

where the coefficients b_0, b_1, and b_2 are given in Table 4.2, and the standard deviation of the curve fit residuals is 0.018%. The same polynomial expression is used to fit the calibration data for the MP and HP CFVs, and their curve fit coefficients are also included in Table 4.2. Lastly, the curve fits shown in Fig. 4.2 agree to better than 0.05 % with data from PTB (flowing air at low flows and natural gas at high flows) and with LADG-LNE (flowing air) [xxii]. This comparison was done using the following nozzles, CFV #2, CFV #3, CFV #4, and CFV #5.

Table 4.2. Calibration Coefficients for LP, MP, and HP CFVs and the Reynolds number range where the fit is valid.

CFV	Re_{MIN}	Re_{MAX}	b_0	b_1	b_2
(-----)	(-----)	(-----)	(-----)	(-----)	(-----)
LP CFVs	1.1×10^6	2.4×10^6	1.101	-3.917	35.683
MP CFVs	3.69×10^6	2.74×10^7	1.0003	-0.1323	0
HP CFVs	3.69×10^6	2.74×10^7	1.0003	-0.1323	0

Uncertainty Analysis of the LP CFVs

When the method of propagation of uncertainty is applied to Eqn. 3.2 (*i.e.*, the calibration equation used for the LP CFVs in Stage 1) the result is[2]

$$\left[\frac{u(C_d)}{C_d}\right]_{LP1}^2 = \left[\frac{u(\dot{m})}{\dot{m}}\right]^2 + \left[\frac{u(P_0)}{P_0}\right]_{LP1}^2 + \frac{1}{4}\left[\frac{u(T_0)}{T_0}\right]_{LP1}^2 + 4\left[\frac{u(d)}{d}\right]_{LP1}^2 + \frac{1}{4}\left[\frac{u(\mathcal{M})}{\mathcal{M}}\right]_{LP1}^2 + \frac{1}{4}\left[\frac{u(R_u)}{R_u}\right]^2 + \left[\frac{u(C_s)}{C_s}\right]_{LP1}^2 + \left[\frac{u\left(C_d^{FIT}\right)}{C_d^{FIT}}\right]_{LP}^2 \quad (4.3)$$

where the subscript "LP1" indicates the Stage 1 LP CFVs, and $\left[u(C_d^{FIT})/C_d^{FIT}\right]$ is the standard deviation of the curve fit residuals. In this expression, the correlations of C_s with P_0 and T_0 have been neglected. In a more exact representation the normalized sensitivity coefficients of P_0 and T_0 would include the appropriate pressure and temperature derivatives of C_s. However, a sensitivity study showed that these dependencies could be omitted with negligible error in both Stages 1 and 2 where the pressure is sufficiently low. On the other hand, we include these dependencies in the uncertainty expressions in Stages 3, 4, and 5 where the pressure is substantially higher. Furthermore, the correlation between P_0 and T_0 (through their common dependence on the specific heat ratio, γ, and on the Mach number, M, [see Eqns. A1 and Eqn. A2 in Appendix A]) affects the uncertainty budget by less than 1×10^{-6} and is ignored.

Table 4.3. Stage 1 Uncertainty Budget for the LP CFV Discharge Coefficient

Unc. Components for Stage 1 LP CFVs	**Rel. Unc. (*k*=1)**	**Sen. Coeff.**	**Perc. Contrib.**	**Unc. Type**	**Comments**
LP CFV Discharge Coeff., C_d = 0.9936	($\times 10^{-6}$)	(-----)	(%)	(A or B)	
PVTt primary standard, ($\dot{m}$ = 675.2 g/s)	450	1.0	79.9	A, B	Based on References [v-vii]
Stag. Pres.; (P_0 = 570.0 kPa)	118	1.0	5.5	A, B	Fit residuals, drift, cal std, etc.
Stag. Temp.; (T_0 = 296.0 K)	176	0.5	3.1	A, B	Spatial Sampling error, drift, fit residuals, etc .
Nominal Throat diameter; (d = 2.54 cm)	0*	2.0	0	B	Nom. value is fixed betwn. Stages 1 and 2
Molar Mass; ($\mathcal{M}$ = 28.9646 g/mol)	25	0.5	0.1	A, B	Variation in air comp. [xix-xxi]
Univ. gas constant; (R_u = 8314.47 J/kmol K)	2	0.5	0.0	A, B	See Reference [xxiii]
Critical Flow Function; ($C_{s,LP}$ =0.6865)	0*	1.0	0	B	Same flow cond. in Stages 1 and 2
CFV Curve Fit Residuals	170	1.0	11.4	A	Fit Residuals, Hysteresis, and Reproducibility
Combined Uncertainty	**503**		**100**		

[2] For convenience, all uncertainty formulas give the square of the actual value unless otherwise noted.

Based on Eqn. 4.3, the Stage 1 uncertainty for the discharge coefficient was 0.05 % with a coverage factor of $k = 1$. The various uncertainty sources are itemized in Table 4.3. The abbreviated titles in the heading of the table, "**Rel. Unc.**", "**Sen. Coeff.**", "**Perc. Contrib.**", and "**Unc. Type**", are taken to mean the following: (1) standard relative uncertainty; (2) normalized sensitivity coefficient; (3) percent contribution of a single component to the overall uncertainty; and (4) the uncertainty type, respectively. By far, the largest component is the relative standard uncertainty of the *PVTt* primary standard (450×10^{-6}). Brief explanations of the remaining uncertainty components are provided in Table 4.3 under the heading "**Comments**".

Throughout this document an asterisk (*) next to an uncertainty value in the "**Rel. Unc.**" column is used to indicate self-canceling measurement errors between adjacent stages. In Table 4.3 the asterisk is used next to the uncertainties for the nominal CFV throat diameter and the critical flow function. Both of these uncertainties are self-canceling since biases introduced in Stage 1 identically cancel with biases of opposite polarity in Stage 2. For example, any bias in the value of the throat diameter used in Stage 1 cancels when the same value of d is used in Stage 2. This argument also applies to the critical flow function since the LP CFVs are used in Stage 2 for the same gas type (*i.e.*, dry air) and at the same nominal conditions (*i.e.*, P_0 and T_0) for which they were calibrated in Stage 1.

4.2 STAGE 2: Calibration and Uncertainty of the MP CFVs

Calibration of the MP CFVs using the LP CFVs

In Stage 2, the four LP CFVs calibrated in Stage 1 are combined in a parallel array and used to calibrate four MP CFVs, one at a time. The calibration setup is shown in Fig. 4.3. Both the downstream LP CFVs and the upstream MP CFV have a CPA 50E flow conditioner[3] installed upstream of their respective pressure and temperature instrumentation. A heat exchanger is used to bring the cold jet exiting the MP CFV back to room temperature conditions before the flow is measured by the array of LP CFVs.

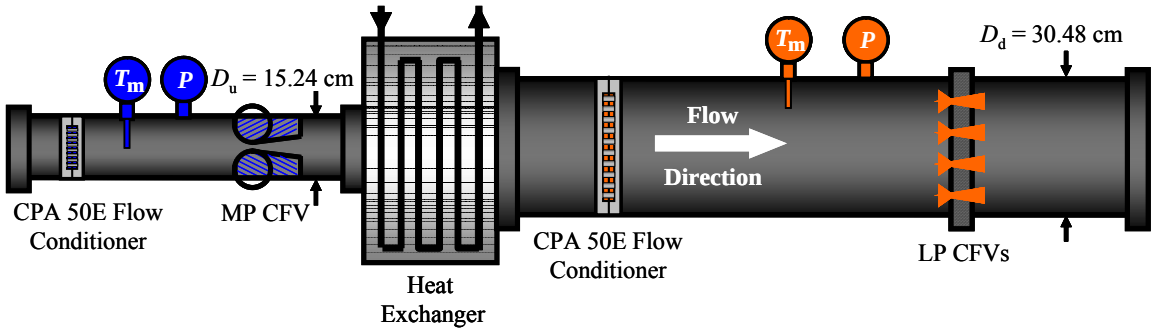

Figure 4.3. Schematic showing the setup for the Stage 2 calibration of the MP CFV using four LP CFVs calibrated in Stage 1 (figure not drawn to scale)

[3] Throughout this document certain commercial equipment, instruments, or materials are identified to foster understanding. Such identification does not imply recommendation or endorsement by the National Institute of Standards and Technology, nor does it imply that the materials or equipment identified are necessarily the best available for the purpose.

The operating conditions for the downstream LP CFVs are controlled so that P_0 and T_0 are nearly equal to their Stage 1 values. Because the working fluid is the same as that in Stage 1 (*i.e.,* dry air), the resulting Reynolds number range corresponds to the values used in the Stage 1 LP CFV calibration. By applying the principle of conservation of mass and using the LP CFVs as working standards, the mass flow through the upstream MP CFV is

$$\dot{m}_{\mathrm{MP2}} = \sum_{\mathrm{n}=1}^{N_2} \dot{m}_{\mathrm{th,n}}^{\mathrm{LP2}} C_{\mathrm{d,n}}^{\mathrm{LP}} + \Delta\dot{m}_2 \tag{4.4}$$

where $N_2 = 4$ is the number of LP CFVs mounted in the downstream nozzle fixture, and $\dot{m}_{\mathrm{th,n}}^{\mathrm{LP2}}$ is the Stage 2 theoretical mass flow for the LP CFVs which is calculated using Eqn. 3.1; and $\Delta\dot{m}_2$ is the rate of mass storage in the connecting volume between the array of LP CFVs and the MP CFV. The mass storage (*i.e.*, line pack) term accounts for density transients in the connecting volume. Because $\Delta\dot{m}_2$ is small relative to $\dot{m}_{\mathrm{MP2}}$, we set $\Delta\dot{m}_2$ equal to zero in Eqn. 4.4; however, the uncertainty attributed to line pack is included in the uncertainty budget.

The calibration procedure begins by establishing steady-state flow conditions at the desired stagnation pressure. Subsequently, pressure and temperature data is collected for approximately 360 s. The data acquisition system cycles at 1.5 Hz, resulting in approximately 540 pressure and temperature data points. At each data point P_0, T_0, C_{s}, and Re are computed at both the LP CFVs and at the MP CFV using the methods explained in Section 3.2 and in Appendix A. These values are used to calculate the MP CFV discharge coefficient

$$C_{\mathrm{d}}^{\mathrm{MP}} \equiv \left[\frac{\dot{m}}{\dot{m}_{\mathrm{th}}}\right]_{\mathrm{MP}} = \sqrt{\frac{T_{0,\mathrm{MP2}}}{T_{0,\mathrm{LP2}}}}\left(\frac{P_{0,\mathrm{LP2}}\, C_{\mathrm{s,LP2}}}{P_{0,\mathrm{MP2}}\, C_{\mathrm{s,MP2}}}\right)\sum_{\mathrm{n}=1}^{N_2}\left(\frac{d_{\mathrm{LP,n}}^2}{d_{\mathrm{MP}}^2}\right) C_{\mathrm{d,n}}^{\mathrm{LP}} \tag{4.5}$$

where the subscripts "LP2" and "MP2" correspond, respectively, to the Stage 2 LP and MP CFVs. The CFV throat diameters are given in Table 3.1, and $C_{\mathrm{d,n}}^{\mathrm{LP}} = C_{\mathrm{d,FIT}}^{\mathrm{LP}}(Re_{\mathrm{LP}})$ is the LP CFV calibration curve given in Eqn. 4.2. The reported $C_{\mathrm{d}}^{\mathrm{MP}}$ values are averaged over the 360 s data collection interval. In the worst case, the standard deviation of the mean for this averaging process is 0.002 %, which is negligible relative to other sources of uncertainty, and is therefore not included in the uncertainty budget.

The $C_{\mathrm{d}}^{\mathrm{MP}}$ values are measured at a minimum of five discrete Re_{MP} values. A minimum of two $C_{\mathrm{d}}^{\mathrm{MP}}$ measurements are made at each of the five Reynolds numbers so that a total of no less than ten measurements are made. A typical calibration begins at the minimum pressure set point, $P_{0,\mathrm{LP2}}$ =375 kPa (or $P_{0,\mathrm{MP2}}$ = 1500 kPa). The set point is increased in equal increments until reaching its maximum value at the fifth pressure set point, $P_{0,\mathrm{LP2}}$ =630 kPa (or $P_{0,\mathrm{MP2}}$ = 2520 kPa). After finishing the fifth data collection, the flow is shutdown (*i.e.*, zero flow) and then reestablished at the maximum set point. The sixth data collection is taken at the maximum set point. The pressure set point is subsequently decreased in equal increments until reaching its minimum value at the tenth set point. This method of collecting data accounts for repeatability, short term reproducibility, and hysteresis effects.

The averaged C_d^{MP} data is depicted in Fig. 4.2 (shown earlier in Section 4.1) where the symbol (●) represents the results of all four MP CFVs. This data set includes a total of 77 points and spans a Reynolds number range from 3.7×10^6 to 8.6×10^6. Unlike the LP CFV data, the MP CFV data is entirely within the turbulent flow regime. Moreover, the entire MP CFV data set can be fit to a single calibration curve

$$C_{d,FIT}^{MP} = b_0 + b_1 \, Re^{-1/5} \tag{4.6}$$

where the coefficients b_0 and b_1 are given in Table 4.2. Considering that the data corresponds to five different CFVs, the small degree of scatter in the data is remarkable; moreover, the standard deviation of the curve fit residuals is only 0.017 %. Perhaps more remarkable is the fact that the same curve also fits the eight HP CFVs in Section 4.3.

Uncertainty Analysis of the MP CFVs

The uncertainty of the MP CFV discharge coefficients is determined by applying the law of propagation of uncertainty to Eqn. 4.5. Because all four LP CFVs are traceable to the same calibration standard, many of their common uncertainty sources are correlated. When these correlations are taken into account, the resulting expression for uncertainty is

$$\begin{aligned}\left[\frac{u(C_d)}{C_d}\right]_{MP}^2 = &\left(\frac{1+r_{LP}(N_2-1)}{N_2}\right)\left[\frac{u(C_d)}{C_d}\right]_{LP}^2 + \left[\frac{u(P_0)}{P_0}\right]_{MP2}^2 + \left[\frac{u(P_0)}{P_0}\right]_{LP2}^2 \\ &+ \frac{1}{4}\left[\frac{u(T_0)}{T_0}\right]_{MP2}^2 + \frac{1}{4}\left[\frac{u(T_0)}{T_0}\right]_{LP2}^2 + 4\left[\frac{u(d)}{d}\right]_{MP2}^2 + 4\left[\frac{u(d)}{d}\right]_{LP2}^2 \\ &+ \left[\frac{u(C_s)}{C_s}\right]_{MP2}^2 + \left[\frac{u(C_s)}{C_s}\right]_{LP2}^2 + \left[\frac{u(C_d^{FIT})}{C_d^{FIT}}\right]_{MP}^2 + u_{IE,2}^2 + \left[\frac{\Delta\dot{m}_2}{\dot{m}_{MP2}}\right]^2\end{aligned} \tag{4.7}$$

where $\left[u(C_d)/C_d\right]_{LP}$ in the first term is the uncertainty for a single LP CFV used by itself. Its uncertainty is determined using Eqn. 4.3 and its value is given in Table 4.3. The uncertainty of all four LP CFVs used together is given by the entire first term, including $\left[u(C_d)/C_d\right]_{LP}$ and the coefficient in parenthesis to which it is multiplied. The coefficient multiplying $\left[u(C_d)/C_d\right]_{LP}$ accounts for the correlation between the four LP CFVs where the correlation coefficient (r_{LP}) specifies the degree of correlation. In the hypothetical case when $r_{LP} = 0$ (*i.e.*, no correlated sources of uncertainty), the coefficient multiplying $\left[u(C_d)/C_d\right]_{LP}$ is $1/N_2$, indicating that the uncertainty of all four LP CFVs used together is less than their individual use. On the other hand, if $r_{LP} = 1$ (*i.e.*, perfectly correlated uncertainty sources), the coefficient multiplying $\left[u(C_d)/C_d\right]_{LP}$ is unity, and there is no difference in uncertainty between using a single LP CFV or multiple LP CFVs together. In the scope of the current work we expect the correlation coefficient to be close to unity since many of the uncertainty sources are correlated. Using the method outlined in reference [xv], we calculated the correlation coefficient to be $r_{LP} = 0.92$.

The last three terms in Eqn. 4.7 are the uncertainties attributed to the standard deviation of the MP CFVs curve fit residuals, $[u(C_{\mathrm{d}}^{\mathrm{FIT}})/C_{\mathrm{d}}^{\mathrm{FIT}}]_{\mathrm{MP}}$; followed by the uncertainty caused by interference effects (*i.e.*, cross-talk) between the four downstream LP CFVs, ($u_{\mathrm{IE},2}$); and lastly the uncertainty attributed to the line packing effect, $[\Delta\dot{m}_2/\dot{m}_{\mathrm{MP2}}]$. The uncertainty attributed to interference effects was measured experimentally by varying the number of open LP CFVs (between two and four) in the nozzle fixture, and comparing the performance to an upstream reference CFV held at constant mass flow. These tests were done on three different occasions and showed that the maximum influence of interference effects was 500×10^{-6}. Assuming a rectangular distribution the standard uncertainty attributed to interference effects is 289×10^{-6}. The uncertainty attributed to the line packing effect was assessed by multiplying the connecting volume by the average rate of density change (in the connecting volume) during the collection. An itemized list of all the uncertainty components along with brief explanations of their uncertainty values are given in Table 4.4.

Table 4.4. Stage 2 Uncertainty Budget for the MP CFV Discharge Coefficient.

Unc. Components for Stage 2 MP CFVs.	**Rel. Unc. (*k*=1)**	**Sen. Coeff.**	**Perc. Contrib.**	**Unc. Type**	**Comments**
MP CFV Discharge Coeff., $C_{\mathrm{d}} = 0.9936$	($\times 10^{-6}$)	(-----)	(%)	(A or B)	
Discharge Coeff. For array of 4 LP CFVs, ($C_{\mathrm{d}}^{\mathrm{LP}} = 0.9936$)	487	1	57.6	A, B	Stage 1 calibration (Corr. effects included)
MP Stag. Pres.; (P_0 = 2280 kPa)	125*	1	3.7	A, B	Uncorr. Unc.: Random Effects, Data Acq., Barometric. Pres.
LP Stag. Pres.; (P_0 = 570 kPa)	129	1	3.9	A, B	Cal. Std., Random Effects, Data Acq., Barometric Pres.
MP Stag. Temp.; (T_0 = 295 K)	230	0.5	3.1	A, B	Cal. Std., Random Effects., Spatial Non-uniformity, etc.
LP Stag. Temp.; (T_0 = 291 K)	241	0.5	3.5	A, B	Cal. Std., Random Effects., Spatial Non-uniformity, etc.
MP Critical Flow Function; ($C_{\mathrm{s,MP}} = 0.6912$)	0*	1	0	A,B	Perfectly correlated betwn. Stages 2 and 3
LP Critical Flow Function; ($C_{\mathrm{s,LP}} = 0.6865$)	0*	1	0	A,B	Perfectly correlated betwn. Stages 1 and 2
Nominal Diameter MP CFV, (d = 2.54 cm)	0*	2	0	B	Perfectly correlated betwn. Stages 2 and 3
Nominal Diameter LP CFV, (d = 2.54 cm)	49*	2	2.3	B	Unc. for thermal expansion betwn. Stages 1 and 2
LP CFV Curve Fit Residuals	170	1	6.9	A	Std. Dev. of Curve Fit Residuals, (see Section 4.1)
Interference effects of multiple CFVs in a Common Plenum	289	1	19.8	B	Exp. varying number of open CFVs in nozzle fixture
Line pack effect	27	1	0.2	B	Based on measured $Vd\rho/dt$ in connecting volume during cal.
Combined Uncertainty	**648**		**100**		

When the uncertainties listed in Table 4.4 are used in Eqn. 4.7 the relative standard uncertainty for $C_{\mathrm{d}}^{\mathrm{MP}}$ is 648×10^{-6} ($k = 1$). As expected, the largest uncertainty contribution derives from the

Stage 1 calibration of the four LP CFVs. The value for this uncertainty (487×10^{-6}) is slightly less than that given in Table 4.3 for the Stage 1 analysis because $r_{LP} < 1$. As discussed in Section 4.1, the asterisk (*) next to selected uncertainty components indicates our assumption that the correlated measurement errors between adjacent stages identically cancel. In the cases where an asterisk is positioned next to the pressure or temperature uncertainties the correlation is caused by the same transducer being used to measure the same nominal conditions in adjacent stages. In this case the listed uncertainties consist entirely of the uncorrelated uncertainty sources. When there is ambiguity as to whether an uncertainty source is perfectly correlated, we conservatively define it to be uncorrelated.

4.3 STAGE 3: Calibration and Uncertainty of the HP CFVs

Calibration of the HP CFVs

In Stage 3 the MP CFVs are configured in parallel and used to calibrate a total of eight HP CFVs, one at a time, in dry air. The calibration setup is similar to the Stage 2 setup shown in Fig. 4.3, but in this case a single HP CFV is positioned upstream of the four MP CFVs configured in parallel. The Stage 3 stagnation pressure at the MP CFVs is controlled so that the Reynolds number overlaps values from the previous calibration stage. The resulting Reynolds number range for the MP CFVs varies from 5.4×10^6 to 7.5×10^6, and the Reynolds number range for the upstream HP CFV varies from 2.0×10^7 to 2.75×10^7. The pressures and flows of the HP CFVs are approximately 16 times the Stage 1 values for the LP CFVs.

The calibration procedure is similar to the calibration of the MP CFVs. After establishing steady state flow conditions in the pipeline, data is collected for approximately 200 s resulting in approximately 270 data points. At each data point we compute P_0, T_0, C_s, and Re at the MP CFVs and at the HP CFV using the methods described in Section 3.1. These values are used to calculate the HP CFV discharge coefficient

$$C_d^{HP} \equiv \left[\frac{\dot{m}}{\dot{m}_{th}}\right]_{HP} = \sqrt{\frac{T_{0,HP3}}{T_{0,MP3}}}\left(\frac{P_{0,MP3}\,C_{s,MP3}}{P_{0,HP3}\,C_{s,HP3}}\right)\sum_{n=1}^{N_3}\left(\frac{d_{MP3,n}^2}{d_{HP3}^2}\right)C_{d,n}^{MP} \tag{4.8}$$

where the subscripts "MP3" and "HP3" correspond, respectively, to the Stage 3 MP and HP CFVs, and $N_3 = 4$ is the number of MP CFVs mounted in the downstream nozzle fixture. The throat diameters of the CFVs are obtained from Table 3.1, and $C_{d,n}^{MP} = C_{d,FIT}^{MP}(Re_{MP})$ is the MP CFV calibration curve given by Eqn. 4.6. The reported C_d^{HP} values are averaged over the 200 s data collection interval. The averaging process introduces negligible uncertainty since in the worst case, the standard deviation of the mean is less than 0.001 %.

For each HP CFV, C_d^{HP} measurements are made at a minimum of three discrete Re_{HP} values. In most cases these measurements were made on two separate occasions so that six measurements are made in total. The format for collecting the data is analogous to the procedure described in Section 4.2. The entire data set for all eight HP CFVs consists of 43 points. The data is shown in Fig. 4.2 (shown earlier in Section 4.1) where the same symbol (■) is used to represent all eight HP CFVs. The eight HP CFVs fit a single calibration curve

$$C_{\mathrm{d,FIT}}^{\mathrm{HP}} = b_0 + b_1\, Re^{-1/5} \tag{4.9}$$

where the coefficients b_0 and b_1 are given in Table 4.2, and the standard deviation of the curve fit residuals is 0.02%.

Uncertainty Analysis of the HP CFVs

The uncertainty of the HP CFVs is determined by applying the method of propagation of uncertainty to Eqn. 4.8. The resulting expression of uncertainty is analogous to Eqn. 4.7 for the MP CFVs

$$\begin{aligned}\left[\frac{u(C_{\mathrm{d}})}{C_{\mathrm{d}}}\right]_{\mathrm{HP}}^2 = {} & \left(\frac{1+r_{\mathrm{MP}}(N_3-1)}{N_3}\right)\left[\frac{u(C_{\mathrm{d,n}})}{C_{\mathrm{d,n}}}\right]_{\mathrm{MP}}^2 + \left[1+\left(\frac{P_0}{C_{\mathrm{s}}}\frac{\partial C_{\mathrm{s}}}{\partial P_0}\right)_{\mathrm{HP3}}\right]^2\left[\frac{u(P_0)}{P_0}\right]_{\mathrm{HP3}}^2 \\ & + \left[\frac{1}{2}-\left(\frac{T_0}{C_{\mathrm{s}}}\frac{\partial C_{\mathrm{s}}}{\partial T_0}\right)\right]_{\mathrm{HP3}}^2\left[\frac{u(T_0)}{T_0}\right]_{\mathrm{HP3}}^2 + \left[\frac{u(P_0)}{P_0}\right]_{\mathrm{MP3}}^2 + \frac{1}{4}\left[\frac{u(T_0)}{T_0}\right]_{\mathrm{MP3}}^2 \\ & + \left[\frac{u(C_{\mathrm{s}})}{C_{\mathrm{s}}}\right]_{\mathrm{HP3}}^2 + \left[\frac{u(C_{\mathrm{s}})}{C_{\mathrm{s}}}\right]_{\mathrm{MP3}}^2 + 4\left[\frac{u(d)}{d}\right]_{\mathrm{HP3}}^2 + 4\left[\frac{u(d)}{d}\right]_{\mathrm{MP3}}^2 \\ & + \left[\frac{u\left(C_{\mathrm{d}}^{\mathrm{FIT}}\right)}{C_{\mathrm{d}}^{\mathrm{FIT}}}\right]_{\mathrm{MP}}^2 + u_{\mathrm{IE,3}}^2 + \left[\frac{\Delta\dot{m}_3}{\dot{m}_{\mathrm{HP}}}\right]^2\end{aligned} \tag{4.10}$$

where in this case the MP CFV correlation coefficient is $r_{\mathrm{MP}} = 0.95$. The normalized sensitivity coefficients for $\left[u(P_0)/P_0\right]_{\mathrm{HP}}$ and $\left[u(T_0)/T_0\right]_{\mathrm{HP}}$ include the pressure and temperature derivatives of C_{s}, respectively. These additional terms take into account the uncertainty in C_{s} attributed to uncertainties in the stagnation conditions. At the lower pressures in Stages 1 and 2 these additional terms made a negligible contribution to the uncertainty and were omitted. However, at the elevated pressures in Stages 3 through 5 they are not negligible and are therefore included.

Table 4.5. Stage 3 Uncertainty Budget for the HP CFV Discharge Coefficient.

Unc. Components for Stage 3 HP CFVs.	**Rel. Unc. (*k*=1)**	**Sen. Coeff.**	**Perc. Contrib.**	**Unc. Type**	**Comments**
HP CFV Discharge Coeff., C_d = 0.9960	($\times 10^{-6}$)	(-----)	(%)	(A or B)	
Discharge Coeff. For array of 4 MP CFVs, (C_d^{MP} = 0.9947)	635	1	56.4	A, B	Stage 2 calibration (Corr. effects included)
HP Stag. Pres.; (P_0 = 9120 kPa)	279	1.03	11.6	A, B	Pres. Cal. Std., Random Effects, Data Acq., Barometric. Pres.
MP Stag. Pres.; (P_0 = 2280 kPa)	123*	1	2.1	A, B	Uncorr. Unc: Random Effects, Data Acq., Barometric Pres. (Corr. Unc. are self-canceling)
HP Stag. Temp.; (T_0 = 295 K)	238	0.64	3.2	A, B	See Reference [xv] (Corr. Unc. are self-canceling)
MP Stag. Temp.; (T_0 = 290 K)	234*	0.5	1.9	A, B	See Reference [xv] (Corr. Unc. are self-canceling)
HP Critical Flow Function; ($C_{s,HP}$ = 0.7097)	215	1	5.8	A,B	Comp. of four Therm. Databases [ii, xxiv-xxvi]
MP Critical Flow Function; ($C_{s,MP}$ = 0.6916)	0*	1	0	A,B	Perfectly correlated betwn. Stages 2 and 3
Nominal Diameter HP CFV, (d = 2.54 cm)	0*	2	0	B	Perfectly correlated betwn. Stages 3 and 4
Nominal Diameter MP CFV, (d = 2.54 cm)	49*	2	1.4	B	Unc. for thermal expansion betwn. Stages 1 and 2
MP CFV Curve Fit Residuals	200	1	5.6	A	Std. Dev. of Curve Fit Residuals, (see Section 4.2)
Interference effects of multiple CFVs in a Common Plenum	289	1	11.7	B	See Section 4.2
Line pack effect	44	1	0.3	B	Based on measured Vdp/dt in connecting volume during cal.
Combined Uncertainty	**849**		**100**		

4.4 STAGE 4: Calibration and Uncertainty of the TMWS

Calibration of the TMWS

In Stage 4 all nine TMWS were individually calibrated in natural gas *at their place of use* and *at their nominal operating conditions*. Each TMWS was calibrated against the HP CFVs that were calibrated in air in Stage 3. The air based calibration can be applied to nozzles flowing natural gas by accounting for real gas effects via the critical flow function, and by matching the Reynolds number. At these high Reynolds numbers (*i.e.*, $Re > 16 \times 10^6$) turbulent CFV theory predicts that the difference between the C_d values for air and natural gas are less than 0.01 % [xxii]. Because the viscosity of natural gas is less than dry air, matching the Reynolds number required that P_0 in the natural gas flow be approximately 20 % lower than its value in dry air. During the calibration process the HP CFVs were maintained below their measured choking pressure ratio (*i.e.*, pressure downstream of the HP CFVs divided by the stagnation pressure) of 0.942.

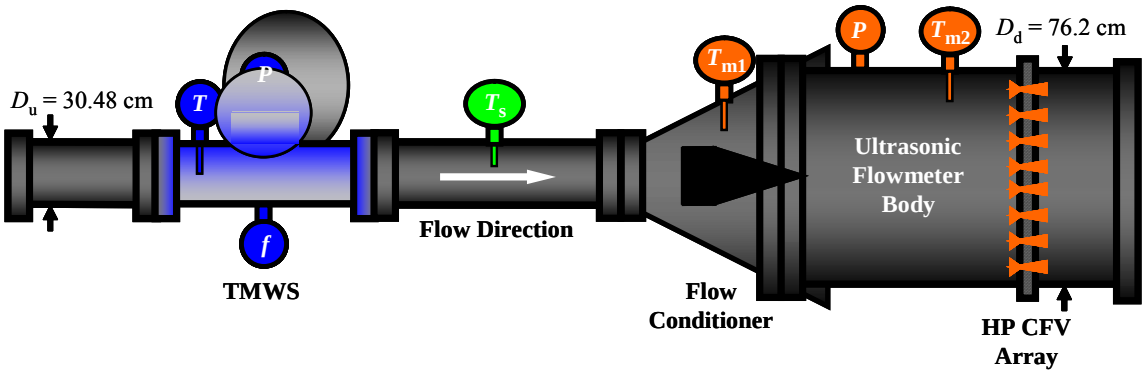

Figure 4.4. Schematic showing the setup for the Stage 4 calibration of the TMWS using the array of HP CFVs calibrated in Stage 3 (*not drawn to scale*)

The TMWS were calibrated twice, once in May 2006, and again in June 2007. A schematic of the calibration setup is shown in Fig 4.4 including the auxiliary pressure, temperature, and frequency measurements. For both tests, redundant instrumentation was used to measure frequency and pressure at the TMWS, and averaged values were used for these two measurements. The temperature at the TMWS was measured with a single resistance temperature device (RTD) installed in a thermowell. Pre-calibration tests showed the maximum effect of the thermowell on the measured temperature was 50.8 mK (0.017 %).

A flow conditioner was installed downstream of the TMWS just before the array of HP CFVs. The conditioner was used to reduce jetting effects as the flow transitions from the smaller 30.48 cm (12 inch) diameter pipeline to the larger 76.2 cm (30 inch) diameter pipeline. Just downstream of the flow conditioner the first temperature measurement (*i.e.*, T_{m1} in Fig. 4.4) was made by averaging the readings of 10 RTDs spaced at equal distances around the circumference of the pipe. The lengths of the RTDs vary so that their penetration depth into the flow stream ranged from 5 cm (*i.e.*, near the pipe wall) to 36 cm (*i.e.*, near the pipe centerline). In this way the temperature was sampled at multiple radii across the cross section. The uncertainty attributed to temperature variation within the cross section was taken to be the standard deviation of the 10 RTDs. Two pipe diameters (D_d) downstream, just before the array of HP CFVs, a second temperature measurement was made (*i.e.*, T_{m2} in Fig. 4.4) using 10 RTDs evenly distributed around the circumference of the pipeline. None of the RTDs at either cross section were installed in thermowells.

Figure 4.5 includes four pictures showing the flow conditioner (A); the calibration setup (B); the 10 RTDs used to measure T_{m2} (C); and the HP CFV array (D). The eight HP CFVs calibrated in Stage 3 were installed in the twenty-one aperture nozzle fixture. The nozzle fixture was installed in the pipeline that houses an ultrasonic flowmeter. Although the ultrasonic flowmeter was not used in the current work it can provide additional temperature information in the future if necessary. To this point, all temperature information was determined using the RTDs. For the May 2006 test only the 10 RTDs that measure T_{m1} were used. The second set of 10 RTDs used to measure T_{m2} were added for the June 2007 tests to determine the uncertainty attributed to axial temperature gradients. The static pressure instrumentation (not shown in Fig. 4.5B) was located approximately one diameter upstream of the HP CFVs on the bottom of the pipe.

Equations 3.1 and 3.2 in Appendix A were used to calculate the stagnation pressure and temperature, respectively.

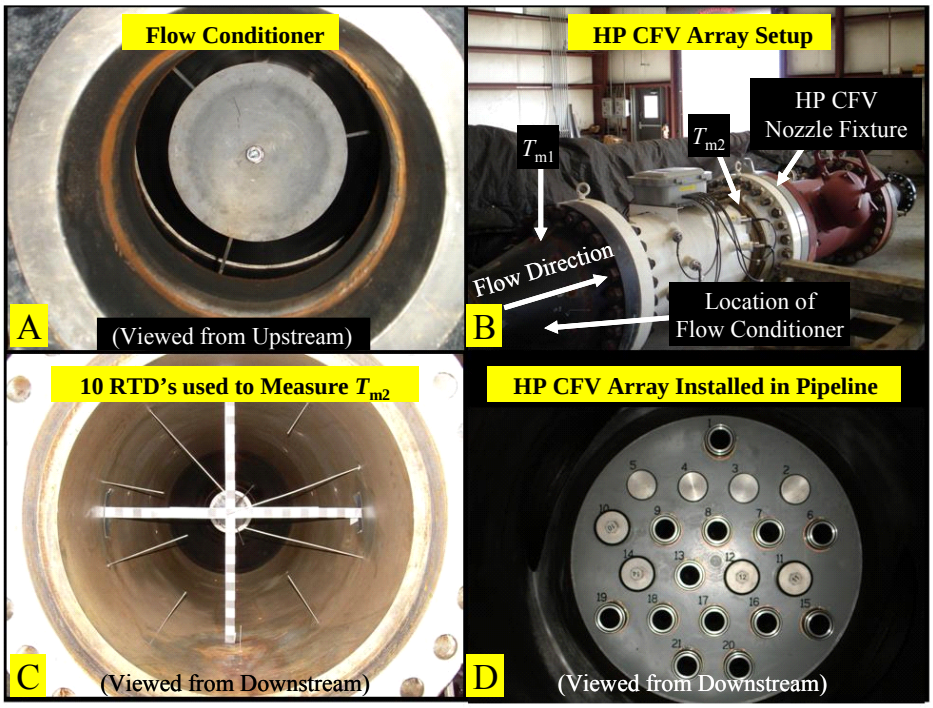

Figure 4.5. Four pictures showing the flow conditioner (A); the configuration of HP CFV array (B); the 10 RTD's used to measure T_{m2} (C); and twenty-one nozzle fixture installed in pipeline (D).

The protocol for calibrating the TMWS is shown in Table 4.6. At the start of the calibration all eight HP CFVs in the nozzle fixture were capped, additional apertures in the nozzle fixture not containing CFVs were sealed, and the TMWS shutoff valves were closed. Subsequently, the pipeline was pressurized to the operating pressure and leak checks are performed. After eliminating any leaks, the end caps were removed from two of the CFVs (*i.e.*, CFV #8 and CFV #17). When steady state conditions were obtained each of the nine TMWS was individually calibrated at the first flow set point. Data was collected for 120 s at each set point, and flow measurements were repeated a minimum of three times at each set point. An additional CFV was uncapped (*i.e.*, opened) at each subsequent set point until all eight HP CFVs were opened as shown in the table. This procedure resulted in each TMWS being calibrated at seven set points over a flow range extending from 0.25 m^3/s (3.2×10^4 acfh) to 1 m^3/s (1.3×10^5 acfh) at a reference temperature near ambient conditions and a reference pressure of approximately 7500 kPa.

Table 4.6. Calibration protocol for the nine TMWS using the eight HP CFVs. Note that the symbol "O" indicates an open CFV (*i.e.*, end cap removed) and the symbol "X" indicates a closed CFV (*i.e.*, end cap securely fastened to divergent section of the CFV). Reference conditions for volumetric flows in the table are at ambient temperature and nominally at 7500 kPa.

Set Point No.	Nominal Flow		No. of Open CFVs	HP CFVs							
(-----)	(m^3/s)	(acfh)	(-----)	CFV #8	CFV #17	CFV #7	CFV #14	CFV #20	CFV #15	CFV #1	CFV #19
1	0.25	3.2×10^4	2	O	O	X	X	X	X	X	X
2	0.375	4.8×10^4	3	O	O	O	X	X	X	X	X
3	0.5	6.4×10^4	4	O	O	O	O	X	X	X	X
4	0.625	7.9×10^4	5	O	O	O	O	O	X	X	X
5	0.75	9.5×10^4	6	O	O	O	O	O	O	X	X
6	0.875	1.1×10^5	7	O	O	O	O	O	O	O	X
7	1	1.3×10^5	8	O	O	O	O	O	O	O	O

Mass conservation can be used to show that the flow at the TMWS being calibrated is

$$q_{\mathrm{TMWS}} = \sum_{\mathrm{n=1}}^{N_4} \frac{\dot{m}_{\mathrm{th,n}}^{\mathrm{HP}} C_{\mathrm{d,n}}^{\mathrm{HP}}}{\rho_{\mathrm{TMWS}}} + \frac{\Delta \dot{m}_4}{\rho_{\mathrm{TMWS}}} \tag{4.11}$$

where N_4 is the number of open HP CFVs which varies between two and eight; $\Delta \dot{m}_4$ is the rate of mass storage in the connecting volume between the TMWS and the nozzle bank; and $\rho_{\mathrm{TMWS}} = [P\mathcal{M}_{\mathrm{gas}} / ZR_{\mathrm{u}}T]_{\mathrm{TMWS}}$ is the density of natural gas at the TMWS where $Z = Z(P,T,x_{\mathrm{k}})$ is the compressibility factor calculated using the REFPROP 8 thermodynamic database [ii] and $\mathcal{M}_{\mathrm{gas}} = \sum x_{\mathrm{k}} M_{\mathrm{k}}$, is the mixture's molar mass. The gas composition (x_{k}) was measured during the testing with an industrial grade gas chromatograph (GC) that was calibrated prior to the testing using a certified gas standard. The theoretical mass flow of the n$^{\mathrm{th}}$ HP CFV ($\dot{m}_{\mathrm{th,n}}^{\mathrm{HP}}$) was determined using Eqn. 3.1. The HP CFV discharge coefficient was determined via the calibration curve fit, $C_{\mathrm{d,n}}^{\mathrm{HP}} = C_{\mathrm{d,FIT}}^{\mathrm{HP}}(Re_{\mathrm{HP}})$, given by Eqn. 4.9 where the throat Reynolds number, (Re_{HP}) was calculated using Eqn. 3.3.

The calibration performance of each of the nine TMWS was determined by the *K*-factor, ($K \equiv f / q_{\mathrm{TMWS}}$) a ratio of the turbine blade frequency (f) divided by volumetric flow (q_{TMWS}). Combining Eqn. 4.11 with the *K*-factor definition yields

$$K = \frac{f}{\frac{\pi}{4}\sqrt{\frac{R_{\mathrm{u}}}{\mathcal{M}_{\mathrm{gas}}}}\left(\frac{P_0 C_{\mathrm{s}}}{\sqrt{T_0}}\right)_{\mathrm{HP}}\left(\frac{ZT}{P}\right)_{\mathrm{TMWS}}\left[\sum_{n=1}^{N_4} d_{\mathrm{HP,n}}^2 C_{\mathrm{d,n}}^{\mathrm{HP}}\right]} \tag{4.12}$$

where $\Delta \dot{m}_4$ from Eqn. 4.11 is set to zero when determining the *K*-factor, but accounted for in the uncertainty budget. Figure 4.6 shows the *K*-factors for all nine TMWS plotted versus the

volumetric flow for the May 2006 data (■) and the June 2007 data (▲). The solid line (——) is a polynomial curve fit of the data

$$K_{\mathrm{FIT}} = c_0 + c_1\, q_{\mathrm{TMWS}} + c_2\, q_{\mathrm{TMWS}}^2 + c_3\, q_{\mathrm{TMWS}}^3 \tag{4.13}$$

where the curve fit coefficients c_0, c_1, c_2, and c_3 are given in Table 4.7.

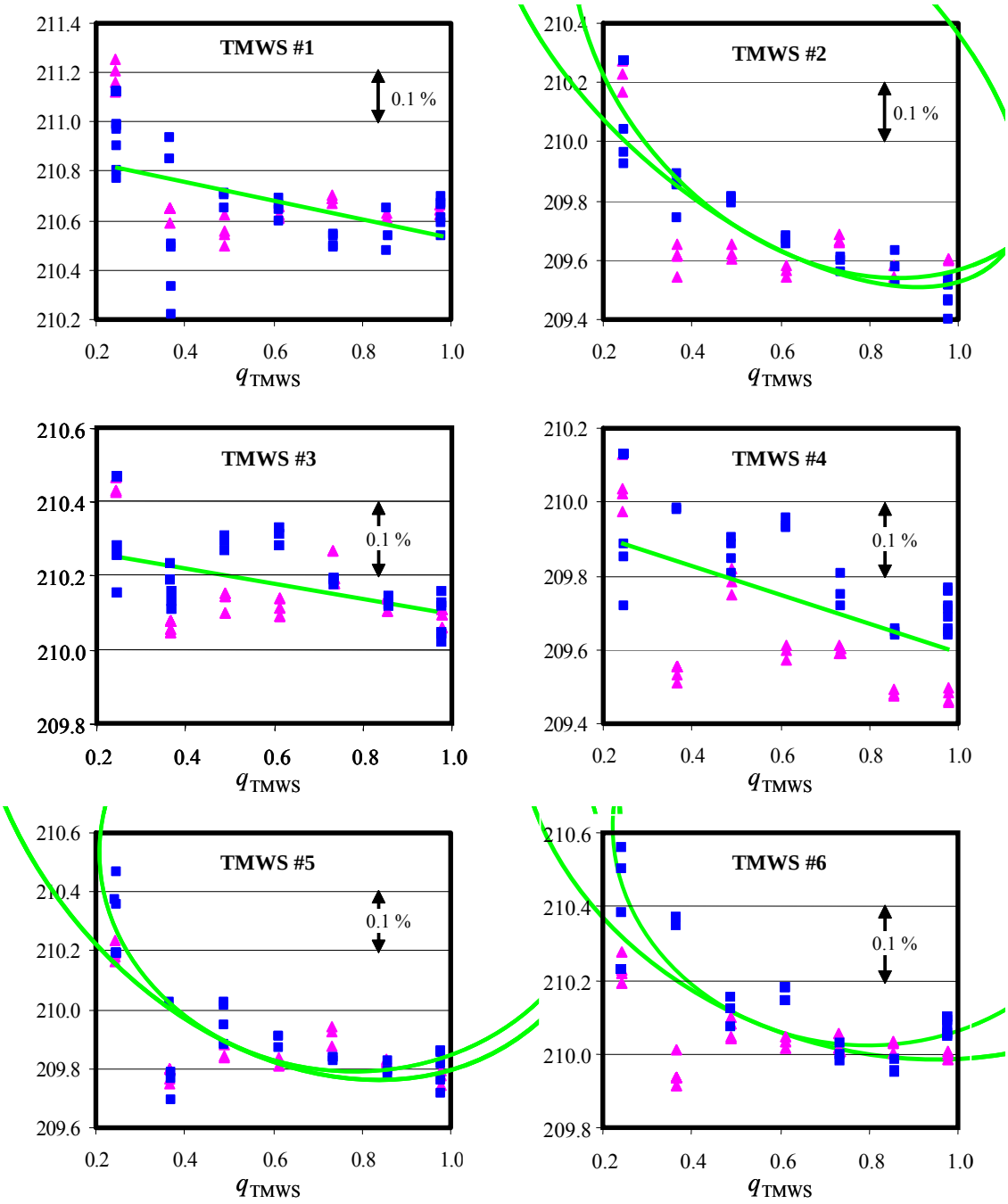

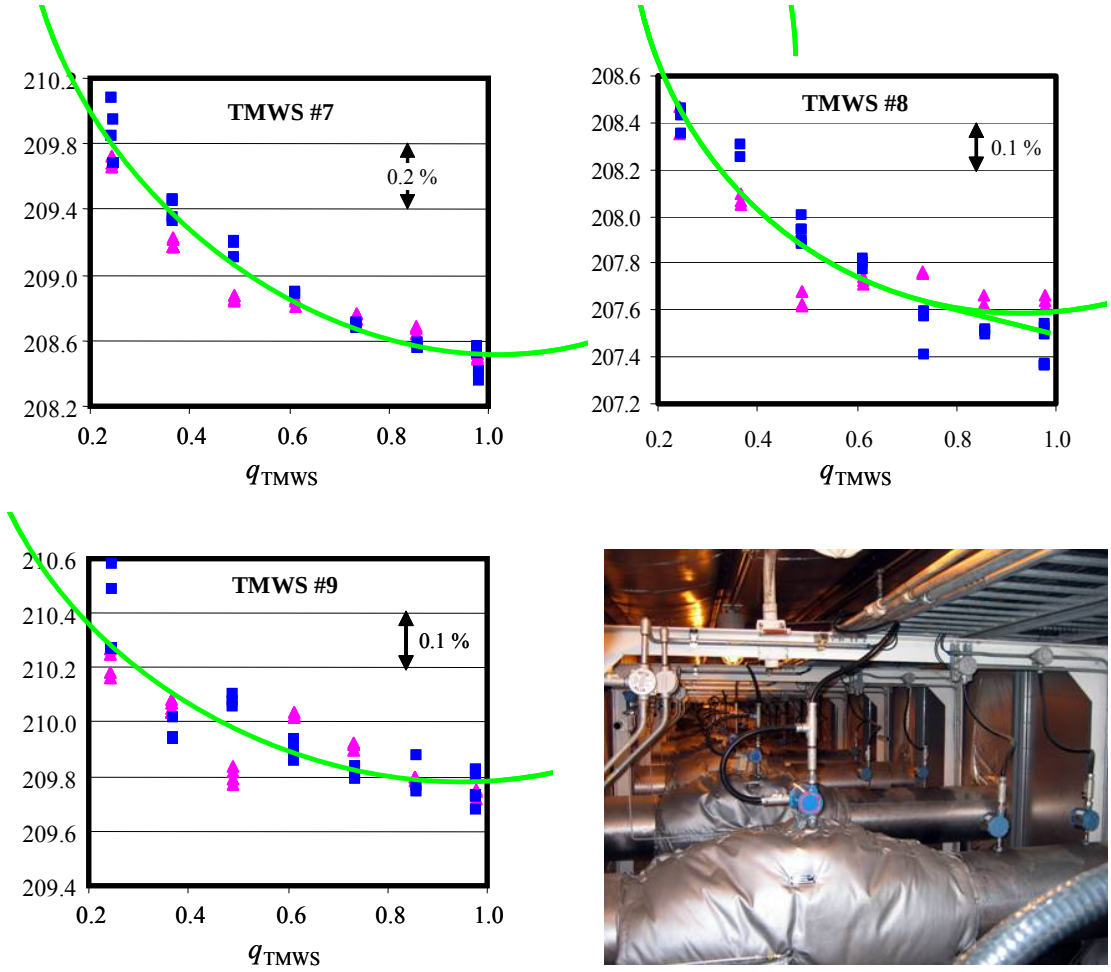

Figure 4.6. *K*-factor (pulse/m^3) calibration curves (——) for all nine TMWS plotted versus volumetric flow (m^3/s) with the squares (■) denoting the May 2006 data and the triangles (▲) signifying the June 2007 data. (The picture at the lower right shows the nine TMWS.)

Table 4.7. Fit coefficients for the *K*-factors of the nine TMWS given in Eqn. 4.13 along with the standard deviation of the fit residuals.

Position Number	TMWS Serial Number	Curve Fit Coefficients				Std. Dev. of Fit Residuals
		c_0	c_1	c_2	c_3	
(-----)	(-----)	(pulse/m^3)	(pulse·s/m^6)	(pulse·s^3/m^9)	(pulse·s^3/m^{12})	(%)
1	97500360	210.911	-0.380	0	0	0.067
2	95380241	210.459	-2.103	1.20	0	0.05
3	97500361	210.306	-0.205	-0.001	0	0.043
4	97500359	209.982	-0.392	0	0	0.067
5	95070034	210.57	-1.99	1.265	0	0.059
6	97310070	210.64	-1.559	0.973	0	0.048
7	94200263	210.692	-4.404	2.233	0	0.056
8	95380242	209.579	-6.208	6.872	-2.753	0.053
9	97470201	210.678	-1.926	1.029	0	0.051

The May 2006 and June 2007 data sets generally showed good agreement, and were well within the *K*-factor measurement uncertainty of 0.24 % to 0.25 %. Excluding TMWS #4, the two sets of data overlap at the majority of flows. In general, the reproducibility between the two data sets (*i.e.*, percent difference of the average *K*-factor's of the May and June data sets) was better at high flows than at lower flows. The larger reproducibility at lower flows could be attributed to problems measuring the lower frequencies in the May data. The larger reproducibility could also in part be caused by temperature stratification in the 70.62 diameter pipeline at the HP CFV array or by line pack (*i.e.*, mass storage effects) resulting from temperature transients in the connecting volume between the TMWS and the HP CFVs. Both of these phenomena are more prevalent at lower flows. In this work we incorporated the uncertainty associated with reproducibility into the calibration curve fit given in Eqn. 4.13. This was done by using both the May 2006 and the June 2007 data in the curve fitting process. On average, the standard deviation of the fit residuals is 0.056 %. The individual values for each TMWS are given in Table 4.7.

The *K*-factors curve fits of the nine TMWS are approximately the same magnitude and generally slope downward with increasing flow. A few of TMWS (*i.e.*, #2, #5, and #6) have *K*-factors that reach a minimum value near 0.8 m^3/s before increasing slightly over the remainder of the calibrated flow range. For both the May 2006 and June 2007 data sets the repeatability (*i.e.*, standard deviation of three or more repeated points at the same nominal flow taken sequentially) generally improved at higher flows. In the May 2006 data set the repeatability was generally 0.02 % at high flows and 0.035 % at low flows. The repeatability of the June 2007 data was generally better than the May 2006 data set, being less than 0.01 % at high flow and approximately 0.02 % at low flows.

Uncertainty Analysis for the Calibration of the TMWS

The uncertainty in the *K*-factor is determined by applying the law of propagation of uncertainty to Eqn. 4.12. The resulting expression for relative uncertainty is

$$\left[\frac{u(K)}{K}\right]^2 = \left(\frac{1+r_{HP}(N_4\text{-}1)}{N_4}\right)\left[\frac{u(C_d)}{C_d}\right]_{HP}^2 + \left[\frac{u(C_s)}{C_s}\right]_{HP4}^2 + \left[\frac{u(Z)}{Z}\right]_{TMWS4}^2 + \left[\frac{u(f)}{f}\right]^2$$

$$+\left(\frac{1}{4}\right)\left[\frac{u(R_u)}{R_u}\right]^2 + 4\left[\frac{u(d_p)}{d_p}\right]_{HP}^2 + u_{tot}^2(M_k) + u_{tot}^2(x_k) + u_{tot}^2(P) \qquad (4.14)$$

$$+u_{tot}^2(T) + \left[\frac{u(K_{FIT})}{K_{FIT}}\right]^2 + u_{IE,4}^2 + u_{unchoke}^2 + u_{species}^2 + \left[\frac{\Delta\dot{m}_4}{\rho_{TMWS}\, q_{TMWS}}\right]^2$$

where the terms $u_{tot}^2(x_k)$, $u_{tot}^2(P)$, $u_{tot}^2(T)$, and $u_{tot}^2(M_k)$ are interim variables, that group together like uncertainty terms. For example, $u_{tot}^2(P)$ is the combined pressure uncertainty for both the TMWS and the HP CFVs. Detailed explanations of these four terms are discussed in Appendix B. The last five terms in Eqn. 4.14 are the following: (1) $\left[u(K_{FIT})/K_{FIT}\right]$ is the standard deviation of the curve fit residuals; (2) $u_{IE,4}$ is the uncertainty attributed to interference (or cross-talk) effects caused by the spacing between the CFVs in the nozzle fixture; (3) $u_{unchoke}$ is the uncertainty attributed to CFV unchoking effects; (4) $u_{species}$ is the uncertainty in the CFV

discharge coefficient attributed to applying the air calibrated CFVs in natural gas at the same Reynolds number; and (5) $\Delta\dot{m}_4$ is the uncertainty attributed to the line packing effect.

The *K*-factor uncertainty decreases slightly with increasing volumetric flow. At the lowest flow (*i.e.*, $N_4 = 2$), the uncertainty is $1\,231 \times 10^{-6}$ for $k = 1$ while at the highest flow (*i.e.,* $N_4 = 8$) the uncertainty decreases to $1\,190 \times 10^{-6}$ for $k = 1$. The decrease in uncertainty at higher flows is a result of several factors including 1) reduced temperature transients in the connecting volume leading to less line pack, 2) reduced spatial temperature gradients in the 76.2 cm diameter pipe immediately upstream of the array of HP CFVs, and 3) a lower uncertainty contribution from the HP CFVs (*i.e.*, the coefficient multiplying $\left[u(C_\mathrm{d})/C_\mathrm{d}\right]_\mathrm{HP}$ in Eqn. 4.14 decreases as N_4 increases).

An itemized list of all of the uncertainty components is provided in Table 4.8 for the highest flow where $q_\mathrm{TMWS} = 1$ m^3/s and $N_4 = 8$. As expected, the largest source of uncertainty (812×10^{-6}) derives from the Stage 3 calibration of the HP CFVs. The uncertainty value given in Table 4.8 for the discharge coefficient of eight CFVs used together is less than the uncertainty given previously in Table 4.5 for a single HP CFV used by itself because $r_\mathrm{HP} < 1$. In particular, the correlation coefficient was calculated to be $r_\mathrm{HP} = 0.91$. A brief description of the uncertainty components are discussed in the table under comments.

Table 4.8. Uncertainty of the TMWS *K*-factor.

***K*-Factor Uncertainty for TMWS**	**Rel. Unc. (*k*=1)**	**Sen. Coeff.**	**Perc. Contrib.**	**Unc. Type**	**Comments**
q_{TMWS} = 1 m^3/s (8 CFVs opened)	(× 10^{-6})	(-----)	(%)	A or B	
Discharge Coefficient, (C_d^{HP} = *0.9936*)	815	-1	46.8	A, B	From Stage 3 unc. anal. (corr. effects incl.)
Critical Flow Function, ($C_{s,NG}$ = *0.7386*)	302	-1	6.4	A, B	See Appendix B
Compressibility Factor, (Z_{TMWS} = *0.8143*)	240	-1	4.1	A, B	See Appendix B
Frequency, (*f* = *45.9254 Hz*)	47	1	0.2	B	Manuf. Spec.
Univ. Gas Constant, (R_u = 8314.472 J/kmol·K)	2	-0.75	0	B	See Reference [xxiii]
Throat diameter, (*d* = *2.5396 cm*)	49*	-2	0.7	B	Unc. for Thermal Expansion between Stages 3 and 4
Total Species Molar Mass Unc.	4.5	1	0	B	Assumed the Std. Unc. of molar mass for various gas comp. is $[u(M_k)/M_k]$=10× 10^{-6}
Total Species Composition Unc.	150	1	1.6	A, B	See Appendix B
Total Pressure Uncertainty	286	1	5.7	A, B	See Appendix B
Total Temperature Uncertainty	336	1	8.0	A, B	See Appendix B
K-factor fit Residuals	560	1	22.1	A	Std. Dev. of Curve Fit Residuals
Interference Effects of multiple CFVs in a common plenum	214	1	3.2	B	Exp. varied spacing of CFVs in nozzle fixture with 21 apertures; (Rect. Dist.)
Unchoking Effects	116	1	0.9	B	Based on unchoking tests done in low pressure air (Rect. Dist.)
CFV Species Effects	58	1	0.2	B	Based on CFV Theory at high Reynolds Number [xxii]
Line Packing Effect	40	1	0.1	B	Based on measured $Vd\rho/dt$ in connecting volume during cal.
Combined Uncertainty	**1191**		**100**		

4.5 STAGE 5: Typical Uncertainty of a Flowmeter Calibration

A description of the Iowa flow facility, the methodology used for measuring volumetric flow, and the flowmeter calibration procedures were described previously in Sections 2.2 through 2.4. This section documents the uncertainty for a typical volumetric flow calibration. Repeatability and reproducibility of the MUT is not included in the analysis. We begin with the equation used for determining the volumetric flow at the MUT

$$q_{MUT} = \left(\frac{\mathcal{M}_{TMWS}}{\mathcal{M}_{MUT}}\right)\sum_{n=1}^{N_5}\left(\frac{P_{TMWS,n}}{P_{MUT}}\right)\left(\frac{T_{MUT}}{T_{TMWS,n}}\right)\left(\frac{Z_{MUT}}{Z_{TMWS,n}}\right)\left(\frac{f_{TMWS,n}}{K_{TMWS,n}}\right) - \frac{\Delta\dot{m}_5}{\rho_{MUT}} \qquad (4.15)$$

given previously by Eqn. 2.8, but repeated here for convenience. In this version of the equation the mass storage effects are included ($\Delta \dot{m}_5$), and the ratio of the TMWS to MUT molar masses are not assumed to cancel. Temporal fluctuations in the gas composition entering the Iowa facility result in a spatial distribution of the mole fraction (x_k) in the piping between the TMWS and the MUT. The difference in x_k at the TMWS and MUT cause $\mathcal{M}_{TMWS}$ and $\mathcal{M}_{MUT}$ to differ. Since the fluctuations are small, this difference can be neglected when calculating q_{MUT}, but should be considered in the uncertainty budget. The uncertainty caused by these fluctuations are typically largest at low flows when the residence time is largest between the TMWS and the MUT.

By applying the method of propagation of uncertainty to Eqn. (4.15) the uncertainty for volumetric flow of a MUT is

$$\left[\frac{u(q)}{q}\right]^2_{MUT} = \left(\frac{1 + r_{TMWS}(N_5 - 1)}{N_5}\right)\left[\frac{u(K)}{K}\right]^2_{TMWS} + \left[\frac{u(f)}{f}\right]^2_{TMWS} + u^2_{tot}(P) + u^2_{tot}(T) + u^2_{tot}(Z) + u^2_{tot}(M_k) + u^2_{tot}(x_k) + \left[\frac{\Delta \dot{m}_5}{\rho_{MUT} q_{MUT}}\right]^2 \quad (4.16)$$

where the correlation coefficient is $r_{TMWS} = 0.92$, and for brevity the total uncertainty of pressure, $u_{tot}(P)$; temperature, $u_{tot}(T)$; the compressibility factor, $u_{tot}(Z)$; species molar masses, $u_{tot}(M_k)$; and gas composition, $u_{tot}(x_k)$; have been grouped together into like terms. The total uncertainties for P, T, and Z include the uncertainties from measurements made both at the MUT and at the array of TMWS, and the total uncertainties for x_k and M_k include the respective uncertainties from all of the constituents in the natural gas mixture.

Table 4.9 provides an itemized list of all of the uncertainty components along with a brief explanation of how it was obtained. For selected components a more detailed explanation is given in Appendix C. The relative uncertainty in the MUT volumetric flow ranges from 1246×10^{-6} at the highest flow (10.7 m^3/s) to 1355×10^{-6} at the lowest flow (0.25 m^3/s). The increased uncertainty at low flows is caused by the increased effect of line packing and by the increased value of the coefficient that multiplies $[u(K)/K]_{TMWS}$ due to a smaller value of N_5.

Table 4.9. Uncertainty of a typical volumetric MUT.

MUT Volumetric Flow Unc.	**Rel. Unc. (*k*=1)**	**Sen. Coeff.**	**Perc. Contrib.**	**Unc. Type**	**Comments**
q_{MUT} = *2.5 m^3/s* (3 TMWS opened)	(× 10^{-6})	(-----)	(%)	A or B	
K-factor, (*K=211.7 pulse/m^3*)	1169	1	86.3	A, B	From Stage 4 unc. anal. (corr. effects incl.)
Total Pressure Uncertainty	263	1	4.4	A, B	Unc. of Pres. Meas. at MUT and TMWS. (see Appendix C)
Total Temperature Uncertainty	351	1	7.7	A, B	Unc. of Temp. Meas. at MUT and TMWS. (see Appendix C)
Frequency, (*f = 91.851 Hz*)	47	1	0.1	A, B	Calibration Records
Total Species Composition Unc.	118	1	0.9	A	Based on Typical Fluctuations in gas composition (see Appendix C)
Total Species Molar. Mass Unc.	0	1	0	B	Perfect correlation betwn. M_k at TMWS & MUT (see Appendix C)
Total Compressibility Factor Unc.	0	1	0	B	Perfect correlation betwn. Z_{MUT} & Z_{TMWS} (see Appendix C)
Line Packing Effect	85	1	0.5	B	Based on Historical $Vd\rho/dt$ in connecting volume during cal.
Combined Uncertainty	**1262**		**100**		

5. SUMMARY AND CONCLUSIONS

This document describes NIST's Natural Gas Flowmeter Calibration Service (NGFCS). Flow calibrations are conducted at the CEESI Iowa natural gas flow facility in Garner, Iowa. However, all flow calibrations are traceable to NIST's low pressure air primary flow standard. Traceability is accomplished in five stages. Figure 3.1 shown earlier in Section 3.1 summarizes the five stage process and list the uncertainty introduced at each stage. The detailed results of this process including flow calibration results and a GUM compliant uncertainty analysis are given in Section 4 of this document.

The expanded uncertainties for volumetric flow calibrations vary from 0.25 % to 0.27 %, increasing at lower flows. The current flow range extends from 1.5×10^4 L/min (3.2×10^4 acfh) to 5.4×10^5 L/min (1.14×10^6 acfh) at a nominal pipeline pressure of 7500 kPa (1088 psi) and at a nominal temperature of 292.5 K (66.8°F). NIST is actively working to both reduce the uncertainty and to extend the lower end of the flow range as discussed in Section 3.3. The NIST website should be consulted for the current capabilities of the NGFCS http://www.cstl.nist.gov/div836/Group_02/index_836.02.html.

REFERENCES

[i] International Organization for Standardization, *General requirements for the competence of testing and calibration laboratories*, ISO/IEC FDIS 17025:2005(E).

[ii] Lemmon, E. W., McLinden, M. O., and Huber, M. L., *REFPROP 23: Reference Fluid Thermodynamic and Transport Properties, NIST Standard Reference Database 23, Version 8*, National Institute of Standards and Technology, Boulder, Colorado, 2007.

[iii] American Gas Association (AGA); *Measurement of Gas by Multipath Ultrasonic Meters*; Transmission Measurement Committee Report No. 9 2nd edition (AGA9), AGA, April 2007.

[iv] Marshall, J. L., *NIST Calibration Services Users Guide, NIST Special Publication 250*, National Institute of Standards and Technology, Gaithersburg, MD, January, 1998.

[v] Johnson, A. N., Wright, J. D., Moldover, M. R., and Espina, P. I, *Temperature Characterization in the Collection Tank of the NIST 26 m^3 PVTt Gas Flow Standard*, Metrologia, 40 (2003), pp. 211-216.

[vi] Johnson, A. N., and Wright, J. D., *Revised Uncertainty Analysis of NIST 26 m^3 PVTt Flow Standard*, Proceedings of the International Symposium on Fluid Flow Measurement, Queretaro, Mexico, (2006).

[vii] Johnson, A. N., Wright, J. D., *Gas Flowmeter Calibrations with the 26 m^3 PVTt Standard*, NIST Special Publication 250-1046, National Institute of Standards and Technology, Gaithersburg, MD, (2006).

[viii] Mickan, B., Kramer, R., Dopheide, D., *Determination of Discharge Coefficient of Critical Nozzles Based on Their Geometry and The Theory of Laminar and Turbulent Boundary Layers*, Proceedings of the International Symposium on Fluid Flow Measurement, Queretaro, Mexico, (2006).

[ix] International Standards Organization, *Measurement of Gas Flow by Means of Critical Flow Venturi Nozzles*, ISO 9300:2005(E).

[x] John, J. E., *Gas Dynamics*, Allyn and Bacon, Inc, 2nd edition, Boston, 1984.

[xi] Stratford, B. S., *The Calculation of the Discharge Coefficient of Profiled Choked* Nozzles and the Optimum Profile for Absolute Air Flow Measurement, Journal Royal Aeron. Soc., Vol. 68, No, 640, April 1964.

[xii] Tang. S., Discharge Coefficients for Critical Flow Nozzles and Their Dependence on Reynolds Numbers, Ph.D. Thesis, Princeton Univ., 1969.

[xiii] Geropp, D., *Laminare Grenzschichten In Ebenen Und RotationssymmetrischenLavalduesen*, Deutsche Luft- Und Raumfart, Forschungsbericht, pp. 71-90, 1971.

[xiv] Taylor, B. N. and Kuyatt C. E., *Guidelines for the Evaluating and Expressing the Uncertainty of NIST Measurement Results*, NIST Technical Note-1297, MD,1994.

[xv] Johnson, A. N. and Kegel, T., *Uncertainty and Traceability for the CEESI Iowa Natural Gas Facility*, J. Res. Natl. Inst. Stand. Technol. 109, 345-369, (2004).

[xvi] Johnson, A. N. and Johansen, B., *U.S. National Standards for High Pressure Natural Gas Flow Measurement*, Proc. of the 2008 Measurement Science Conference, Anaheim, CA (2008).

[xvii] Coleman, H. W., and Steele, W. G., *Experimentation and Uncertainty Analysis for Engineers*, John Wiley and Sons, Inc., New York, NY, 1989.

[xviii] Taylor, B. N. and Kuyatt C. E., Guidelines for the Evaluating and Expressing the Uncertainty of NIST Measurement Results, NIST TN-1297, MD,1994.

[xix] J. Hilsenrath, C. W. Beckett, W. S. Benedict, L. Fano, H. J. Hoge, J. F. Masi, R. L. Nuttall, Y. S. Touloukian, H. W. Wooley, *Tables of Thermal Properties of Gases*, U.S. Department of Commerce NBS Circular 564, 1955.

[xx] Weast, R. C., *CRC Handbook of Chemistry and Physics,* CRC Press Inc., 58th edition, Ohio, 1977.

[xxi] Mackenzie, F. T. and Mackenzie, J. A., *Our changing planet*. Prentice-Hall, Upper Saddle River, NJ, p 288-307, 1995 (After Warneck, 1988; Anderson, 1989; Wayne, 1991.)

[xxii] Mickan, B., Kramer, R., Dopheide, D., Hotze, H., Hinze, H., Johnson, A, Wright, J., Vallet, J.-P., *Comparisions by PTB, NIST, and LNE-LADG, in Air and Natural Gas with Critical Venturi Nozzles Agree within 0.05 %,* Proceedings of the International Symposium on Fluid Flow Measurement, Queretaro, Mexico, (2006).

[xxiii] Moldover, M. R., Trusler, J. P. M., Edwards, T. J., Mehl, J. B., and Davis, R. S., *Measurement of the Universal Gas Constant R Using a Spherical Acoustic Resonator*, NIST J. of Res., 93, (2), 85–143, 1988.

[xxiv] American Gas Association (AGA); *Compressibility Factor of Natural Gas and Other Related Hydrocarbon Gases*, AGA Transmission Measurement Committee Report No. 8 (AGA8), 1994.

[xxv] Kunz, O., Klimeck, R., Wagner, W., and Jaeschke, M. The GERG-2004 Wide-Range Equation of State for Natural Gases and Other Mixtures,GERG TM15, 2007.

[xxvi] Lemmon, E. W., McLinden, M. O., and Huber, M. L., *NIST Standard Reference Database 23: Reference Fluid Thermodynamic and Transport Properties-REFPROP Version 7*.0 National Institute of Standards and Technology, Standard Reference Data Program, Gaithersburg, 2002.

[xxvii] Johnson, R. C., *Calculations of Real-Gas Effects in Flow Through Critical Nozzles*, Journal of Basic Engineering, September 1964, pp. 519.

[xxviii] McLinden, M. O., and Cornelia, L., *Apparatus for wide-ranging, high-accuracy fluid (p,ρ,T) measurements based on a compact two-sinker densimeter,* J. Chem. Thermodynamics 39 (2007) 507–530

[xxix] Boggs, P. T., et. al., *User's Reference Guide for ODRPACK Version 2.01 -- Software for Weighted Orthogonal Distance Regression*, NIST IR 4834*,* U.S. Government Printing Office, 1992.

[xxx] Boggs, P. T., et. al., *Orthogonal Distance Regression*, Contemporary Mathematics, Volume 112: Statistical Analysis of Measurement Error Models and their Applications*,* P. J. Brown and Wayne A. Fuller, Editors, pp. 183-194, American Mathematical Society, Providence, Rhode Island, 1990.

APPENDIX A: CFV Calculations

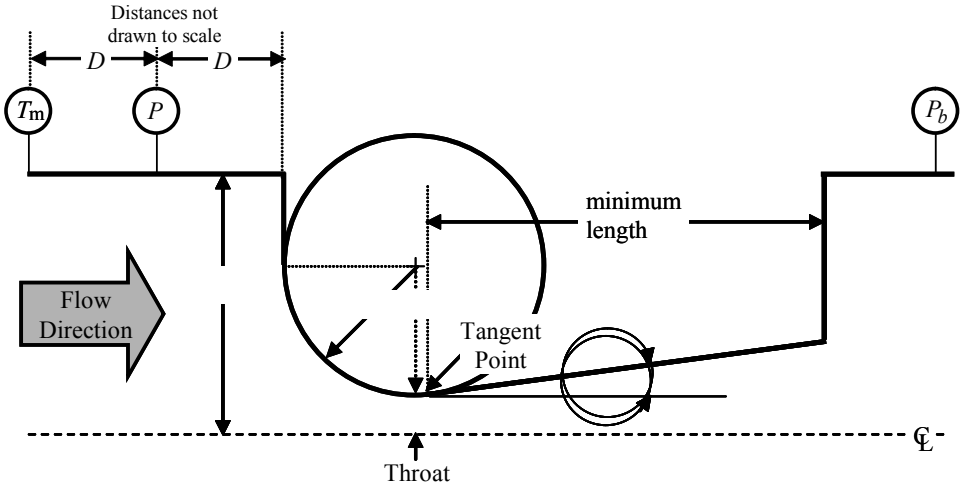

Figure A1. Cross sectional cut of a toroidal shaped ISO 9300 CFV **[ix]**

Figure A.1 shows an cross sectional cut of a toroidal throat CFV. The CFV profile consists of a circular arc extending slightly beyond the throat cross section to a point of tangency, followed by a conical divergent section with a half angle between 2 and 6 degrees. As shown in the figure the static pressure, P, is measured one pipe diameter (D) upstream of the CFV inlet while the temperature, T_m, is measured with a either a thermistor or RTD two pipe diameters upstream of the inlet. The static pressure is used to calculate the stagnation pressure

$$P_0 = P\left[1+\left(\frac{\gamma-1}{2}\right)M^2\right]^{\frac{\gamma}{\gamma-1}}, \tag{A1}$$

where $\gamma = C_p/C_v$ is the specific heat ratio evaluated at the measured temperature and pressure, and M is the Mach number in the approach pipe, and the stagnation temperature is calculated using

$$T_0 = T_m\left[1+\left(\frac{\gamma-1}{2}\right)M^2(1-r)\right] \tag{A2}$$

where $r = 0.75$ is the recovery factor, a parameter accounting for the viscous heating that occurs as the gas irreversibly comes to rest on surface of the temperature probe. The accuracies of Eqns. A1 and A2 increase at lower Mach numbers. For the largest Mach numbers in this work ($M < 0.016$) the difference between P and P_0 is less than 0.019 % while for T_m and T_0 the difference is less than 0.002 %. Consequently, more than 99 % of the uncertainty in P_0 and T_0 derive from P and T_m, respectively, and uncertainty contributions from γ, M, and r can be neglected.

The freestream Mach number can be calculated using either of the two methods. When the mass flow, $\dot{m}$, through the CFV is known (*i.e.*, the CFV is being calibrated), the Mach number can be calculated using

$$M \equiv \frac{u}{c} = \frac{4\dot{m}}{\pi \rho D^2 c} \tag{A3}$$

where u is average flow velocity in approach pipe, and ρ and c are the gas density and sound speed, respectively. On the other hand, when the CFV is being used to determine $\dot{m}$ the Mach number can be determined by inverting the following expression

$$\beta^2 = M\left[\left(\frac{2}{\gamma+1}\right)\left(1+\left(\frac{\gamma-1}{2}\right)M^2\right)\right]^{(\gamma+1)/(2-2\gamma)} \tag{A4}$$

derived from one-dimensional compressible flow theory [x] where $\beta \equiv d/D$. To avoid inverting Eqn. A4 we used the following low Mach number approximation

$$M = \frac{1}{\beta^2}\left(\frac{2}{\gamma+1}\right)^{(\gamma-3)/(2\gamma-2)}\left[1-\sqrt{1-2\beta^4\left(\frac{2}{\gamma+1}\right)^{2/(\gamma-1)}}\right] \tag{A5}$$

which for $\beta < 1/6$ (as in this work) introduces a negligible error (*i.e.*, less than 0.000001 %).

Virial effects in CFV flows are accounted for by the real gas critical flow function

$$C_s = \frac{\rho_t a_t \sqrt{R_u T_0}}{P_0 \sqrt{\mathcal{M}}}. \tag{A6}$$

This thermodynamic property is computed numerically by integrating along an adiabat to determine the density (ρ_t) and sound speed (a_t) at the CFV throat [xxvii]. These integrations were conducted using the REFPROP 8 Thermodynamic Database [ii].

APPENDIX B: Analysis of Selected Stage 4 Uncertainty Components

Appendix B supports the uncertainty analysis of the nine TMWS in Section 4.4. These TMWS were calibrated against an array of HP CFVs shown in Fig. 4.4 and the *K*-factor was determined by Eqn. 4.12. The uncertainty of the *K*-factor was determined by Eqn. 4.14, derived using the GUM procedure [xiv]. Table 4.8 gives numerical values for the uncertainty components in this equation. Additional details are provided below for the following five uncertainty components: 1) $u_{\text{tot}}(P)$, the total pressure uncertainty; 2) $u_{\text{tot}}(T)$, the total temperature uncertainty; 3) $u_{\text{tot}}(M_{\text{k}})$, the total uncertainty of the species molar masses; 4) $\left[u(Z)/Z\right]_{\text{TMWS}}$, the uncertainty of the compressibility factor; 5) $u_{\text{tot}}(x_{\text{k}})$ the total uncertainty attributed to the measured gas composition.

Table B1. Uncertainty of the two pressure transducers used to measure the average pressure at the TMWS

Unc. of TMWS Pressure	**Abs. Unc.**	**Rel. Unc. (*k*=1)**	**Perc. Contrib.**	**Unc. Type**	**Comments**
TMWS Pressure, P = 7500 kPa	(Pa)	(× 10^{-6})	(%)	A or B	
Uncorrelated Unc.					
Short Term Random Uncertainty	270.1	38	2.4	A	Calibration Control Charts
Long Term Random Uncertainty	1556.3	217	78.8	A	Calibration Control Charts
Data Acquisition (Agilent 34970A)	331.3	46	3.6	B	Manuf. spec.
Correlated Unc.					
Dead Weight Pressure Standard (Ametek EPC 2000)	414.2	58	5.6	B	Based on Manuf. Calibration
Ambient Temperature Effect	543.8	76	9.6	B	Manuf. spec.
Transducer mounting orientation	0.0	0	0.0	B	Calibrated and used in the same mounting position
Propagation of Uncorrelated Sources	***1614***	***225***	***84.8***		
Propagation of Correlated Sources	***684***	***95***	***15.2***		
Combined Uncertainty	**1753**	**244**	**100**		

Total Pressure Uncertainty: $u_{\text{tot}}(P)$

Pressure measurements were made both at the TMWS being calibrated and at the array of HP CFVs as shown in Fig. 4.4 of Section 4.4. The pressure at the TMWS was measured using two transducers, and the recorded pressure was the average of the two readings. Likewise, the pressure at the array of HP CFVs was also measured using two transducers. All four transducers were calibrated by the same pressure standard. Moreover, the nominal pressures at both the TMWS and at the array of HP CFVs were identical. Since the transducers were used to measure the same conditions and are traceable to the same standard, some of their uncertainty sources are correlated. Tables B1 and B2 itemize both the correlated and uncorrelated uncertainty sources corresponding to measurements at the TMWS and at the HP CFVs respectively. The standard uncertainties are $\left[u(P)/P\right]_{\text{TMWS}} = 244\times 10^{-6}$ at the TMWS and $\left[u(P_0)/P_0\right]_{\text{HP}} = 200\times 10^{-6}$ at the array of HP CFVs.

APPENDIX B: Analysis of Selected Stage 4 Uncertainty Components

The expression for the total pressure uncertainty, $u_{\text{tot}}(P)$, is derived using the propagation of uncertainty

$$u_{\text{tot}}^2(P) = \left[1+\left(\frac{P_0}{C_s}\frac{\partial C_s}{\partial P_0}\right)\right]^2\left[\frac{u(P_0)}{P_0}\right]_{\text{HP}}^2 + \left[1-\left(\frac{P}{Z}\frac{\partial Z}{\partial P}\right)_{\text{TMWS}}\right]^2\left[\frac{u(P)}{P}\right]_{\text{TMWS}}^2 - 2\left[1+\left(\frac{P_0}{C_s}\frac{\partial C_s}{\partial P_0}\right)\right]\left[1-\left(\frac{P}{Z}\frac{\partial Z}{\partial P}\right)_{\text{TMWS}}\right]\left[\frac{u_c(P_0)}{P_0}\right]_{\text{HP}}\left[\frac{u_c(P)}{P}\right]_{\text{TMWS}} \quad \text{(B1)}$$

where the first two terms include the standard pressure uncertainties at the HP CFV array and the TMWS, and the last term accounts for the correlated uncertainties, $[u_c(P_0)/P_0]_{\text{TMWS}} = 95 \times 10^{-6}$ and $[u_c(P_0)/P_0]_{\text{HP}} = 95 \times 10^{-6}$, listed in Tables B1 and B2 respectively. The derivative expressions in Eqn. B1 are computed numerically using finite difference methods. Based on Eqn. (B1) the total relative pressure uncertainty equals $u_{\text{tot}}(P) = 243 \times 10^{-6}$ for $k = 1$.

Table B2. Uncertainty of two pressure transducers used to measure the average pressure at the array of HP CFVs

Unc. of Pressure at HP CFV Array	**Abs. Unc.**	**Rel. Unc. (*k*=1)**	**Perc. Contrib.**	**Unc. Type**	**Comments**
HP CFV Stag. Pressure, P_0 = 7500 kPa	(Pa)	(× 10^{-6})	(%)	A or B	
Uncorrelated Unc.					
Short Term Random Uncertainty	408.9	57	8.1	A	Calibration Control Charts
Long Term Random Uncertainty	1143.0	159	63.5	A	Calibration Control Charts
Data Acquisition (Agilent 34970A)	331.4	46	5.4	B	Manuf. spec.
Dynamic Pressure	84.7	12	0.3	B	Sensitivity Study: Calc. P_0 based on Eqn (A1) assuming [u(M)/M]= 10 % & [u(γ)/γ]= 5 %
Correlated Unc.					
Dead Weight Pressure Standard (Ametek EPC 2000)	414.2	58	8.3	A, B	Based on Manufactures Calib.
Ambient Temperature Effect	543.8	76	14.4	B	Manuf. spec.
Transducer mounting orientation	0.0	0	0	B	Always in same mounting position
Propagation of Uncorrelated Sources	***1261***	***176***	***77.3***		
Propagation of Correlated Sources	***684***	***95***	***22.7***		
Combined Uncertainty	**1435**	**200**	**100**		

Total Temperature Uncertainty: $u_{\text{tot}}(T)$

Temperature measurements were made both at the TMWS and at the array of HP CFVs as shown previously in Fig. 4.4 of Section 4.4. At the TMWS temperature was measured using a single RTD installed in a thermowell. Prior to starting the flow calibration tests we expereimentally characterized the temperature uncertainty attributed to the thermowell. These tests were done at

the lowest flow when end conduction effects are largest due to reduced convection heat transfer. The standard uncertainty due to the thermowell was 172×10^{-6} (or 50 mK).

The pipe diameter upstream of the HP CFVs is 2.5 times the size of the pipe diameter at the TMWS. Since the gas density is nearly the same in both sections of pipe, the velocity in the approach piping of the HP CFV is lower than the velocity at the TMWS by a factor of nearly 6.25. The low gas velocity upstream of the HP CFVs (*i.e.*, ranging from 0.5 m/s to 2 m/s) causes a spatial temperature distribution in the gas due to stratification. To account for spatial temperature variations we measured the temperature at two axial locations in the pipe indicated by T_{m1} and T_{m2} in Fig. 4.4. Both T_{m1} and T_{m2} are the average of 10 RTDs spaced evenly around the pipe circumference. The lengths of the RTDs vary so that their insertion depths into the flow stream span multiple radii within the cross section as shown in Fig. 4.5C. Another temperature measurement indicated by T_s in Fig. 4.4 is made using a single RTD located $8\,D_d$ upstream of the HP CFV array in the 30.48 cm diameter pipeline. None of the RTDs used to measure T_{m1}, T_{m2}, or T_s are installed in thermowells.

The configuration of RTDs used to measure the temperature upstream of the HP CFV array are used to assess the uncertainty attributed to spatial temperature variations in the gas both in the cross sectional and axial directions. The uncertainty attributed to cross sectional temperature variation is taken to be the standard deviation of the 10 RTDs while the uncertainty in the axial direction is determined by comparing T_{m1}, T_{m2}, and T_s.

Table B3. Uncertainty of temperature (T_{TMWS}) at the TMWS

Unc. of TMWS Temperature	**Abs. Unc.**	**Rel. Unc. (*k*=1)**	**Perc. Contrib.**	**Unc. Type**	**Comments**
Temp. at TMWS, T = 295 K	(mK)	($\times 10^{-6}$)	(%)	A or B	
Uncorrelated Unc.					
Fit Residuals/Reproducibility	13.1	44	3.4	A	Calibration Control Charts
Effect of Thermowell	50.8	172	50.6	B	RTD Exp. with and w/o Thermowell
Data Acquisition (Agilent 34970A)	17.5	60	6	B	Manuf. spec.
Temp. Non-uniformity	30	102	17.7	B	Comparison with nearby RTD
RTD Self Heating	31.7	107	19.7	B	Exp. varied current
Correlated Unc.					
Temperature Transfer Standard	5.8	20	0.7	B	Calibration by Manuf.
Ambient Temperature Effect	5.3	18	0.5	B	Manuf. Spec.
100 Ohm Standard Resistor	8.6	29	1.4	A	Std. Dev. of 3 Calibration
Propagation of Uncorrelated Sources	***70.5***	***239***	***97.4***		
Propagation of Correlated Sources	***11.6***	***39***	***2.6***		
Combined Uncertainty	**71.4**	**242**	**100**		

APPENDIX B: Analysis of Selected Stage 4 Uncertainty Components

Two sets of TMWS flow calibrations were done, the first in May 2006 and the second in June 2007. The second temperature T_{m2} was not measured in the May 2006 test. In this test, the axial temperature uncertainty was estimated by comparing T_{m1} to T_s. On average, the difference between these temperatures was less than 12 mK. The small difference indicated that the measured temperature, T_{m1}, is a reliable estimate of the true average temperature, in spite of the standard deviation of the 10 RTDs being, on average, 151 mK.

In the June 2007 tests three temperatures, T_{m1}, T_{m2} and T_s, were used to assess the axial temperature differences. These three temperatures agreed to within 20 mK or better, except at the lowest flow (*i.e.*, 0.25 m^3/s) where the difference between T_{m1} and T_{m2} exceeded 100 mK. The two sets of 10 RTDs used to measured T_{m1} and T_{m2}, respectively, were used assess the size of temperature differences at two cross sections upstream of the HP CFV array. At high flows the standard deviations of the 10 RTDs used to measure T_{m1} and T_{m2} were both 15 mK, while at low flows the standard deviations were 120 mK and 78 mK respectively.

Table B4. Uncertainty stagnation temperature ($T_{0,HP}$) at HP CFV Array

Unc. of HP CFV Temperature	**Abs. Unc.**	**Rel. Unc. (*k*=1)**	**Perc. Contrib.**	**Unc. Type**	**Comments**
HP CFV Stag. Temp., T_0=295 K	(mK)	($\times 10^{-6}$)	(%)	A or B	
Uncorrelated Unc.					
Fit Residuals/Reproducibility	13.1	44	4	A	Calibration Control Charts
Data Acquisition (Agilent 34970A)	17.5	60	7.1	B	Manuf. spec. (Rect. Dist.)
Axial Temperature Differences	20.2	69	9.4	B	Diff. betwn. T_{m2} and T_{m1} with 8 HP CFVs opened
Cross sectional Temperature Differences	47.9	162	53.1	A	Std. Dev. of 10 RTD's with 8 HP CFVs opened
RTD Self Heating	31.7	107	23.2	B	Exp. varied current
Stag. vs. meas. Temp.	0.7	3	0	B	Sensitivity Study: Calc. T_0 based on Eqn (A2) assuming [u(M)/M]= 10 % & [u(γ)/γ]= 5 %
Correlated Unc.					
Temperature Transfer Standard (Ametek EPC 2000)	5.8	20	0.8	A, B	Manuf. Calibration
Ambient Temperature Effect	5.3	18	0.6	B	Manuf. spec. (Rect. Dist.)
100 Ohm Standard Resistor	8.6	29	1.7	A	Based on Calibration
Propagation of Uncorrelated Sources	***65.8***	***223***	***97.0***		
Propagation of Correlated Sources	***11.6***	***39***	***3.0***		
Combined Uncertainty	**67**	**227**	**100**		

The uncertainty components for the single RTD installed at the TMWS, and for both sets of 10 RTDs installed upstream of the array of HP CFVs are listed in Tables B3 and B4, respectively.

APPENDIX B: Analysis of Selected Stage 4 Uncertainty Components

The uncertainty components are categorized into correlated and uncorrelated sources. In this case the correlated sources of uncertainty result from the RTDs being traceable to the same temperature standard, and from the standard resistor in the current loop used to measure temperature. Applying the method of propagation of uncertainty, the total temperature uncertainty is

$$u_{\mathrm{tot}}^2(T) = \left[\frac{1}{2} - \left(\frac{T_0}{C_\mathrm{s}}\frac{\partial C_\mathrm{s}}{\partial T_0}\right)\right]^2\left[\frac{u(T_0)}{T_0}\right]_{\mathrm{HP}}^2 + \left[1 + \left(\frac{T}{Z}\frac{\partial Z}{\partial T}\right)\right]^2\left[\frac{u(T)}{T}\right]_{\mathrm{TMWS}}^2$$
$$- 2\left[\frac{1}{2} - \left(\frac{T_0}{C_\mathrm{s}}\frac{\partial C_\mathrm{s}}{\partial T_0}\right)\right]\left[1 + \left(\frac{T}{Z}\frac{\partial Z}{\partial T}\right)\right]\left[\frac{u_\mathrm{c}(T_0)}{T_0}\right]_{\mathrm{HP}}\left[\frac{u_\mathrm{c}(T)}{T}\right]_{\mathrm{TMWS}} \qquad \text{(B2)}$$

where the first two terms, $[u(T)/T]_{\mathrm{TMWS}} = 242 \times 10^{-6}$ and $[u(T_0)/T_0]_{\mathrm{HP}} = 227 \times 10^{-6}$, are the standard temperature uncertainties at the TMWS and HP CFV array, and $[u_\mathrm{c}(T)/T]_{\mathrm{TMWS}} = 27 \times 10^{-6}$ and $[u_\mathrm{c}(T)/T]_{\mathrm{TMWS}} = 27 \times 10^{-6}$ in the last term are the correlated uncertainties. The derivative sensitivity coefficients are calculated numerically using finite differences. Using Eqn. B2 with the appropriate uncertainty components in Tables B3 and B4 the total standard temperature uncertainty is $u_{\mathrm{tot}}(T) = 339 \times 10^{-6}$ (k = 1).

Uncertainty of the Compressibility Factor: $u_{\mathrm{tot}}(Z)$

The compressibility factor was computed using the REFPROP 8 Thermodynamic Database. In general, the uncertainty of the compressibility factor for this equation of state can range from 0.02 % to 0.1 % ($k = 2$) depending on the constituents of the natural gas mixture, as well as the specific pressure and temperature used to evaluate Z. In the present work we determined the uncertainty of the REFPROP 8 compressibility factor (Z_{R8}) for natural gas compositions corresponding to the Iowa flow facility (see Table 2.1 of Section 2.1) at typical pipeline pressures of 7500 kPa and at ambient temperature conditions. The uncertainty was assessed by comparing values of the compressibility factor calculated with the REFPROP 8 Database (Z_{R8}) to experimentally measured (Z_{meas}) at the same conditions. The comparison was done using gas samples extracted from the Iowa flow facility. The compressibility factor of gas samples obtained from the Iowa flow facility was measured at two pressures along an isotherm of 298.15 K. These measurements were made near the minimum (6837 kPa) and maximum (8018 kPa) operating pressures of the Iowa facility.

The compressibility factor measurements were done by NIST Physical and Chemical Properties Division using a two sinker densimeter [xxviii]. A three step process was implemented to determine Z_{meas}. In the first step, the density of the gas sample was measured at the two pressures of interest (6837 kPa and 8018 kPa) at 298.15 K. Next, the density of the sample gas was determined at multiple lower pressures ranging from 600 kPa to 3000 kPa at 298.15 K. The low pressure data was fit to the virial equation of state with the molar mass ($\mathcal{M}$) treated as an unknown constant that was determined by the regression analysis, $P/\rho R_\mathrm{u} T = 1/\mathcal{M} + \rho\hat{B} + \rho^2\hat{C} + \rho^3\hat{D}$. The virial coefficients (which herein are divided by the molar mass, $\hat{B} \equiv B/\mathcal{M}$, $\hat{C} \equiv C/\mathcal{M}$, and $\hat{D} \equiv D/\mathcal{M}$) were also determined by the regression

analysis. The curve fit used density as the independent variable so that the point of zero density (*i.e.*, the ideal gas limit) was inversely proportional to $\mathcal{M}$. The random uncertainties associated with this fitting process were determined using the ODR regression package [xxix, xxx]. Systematic uncertainties related to biases in the measurements of density, pressure, and temperature were considered separately. The total uncertainty in $\mathcal{M}$ was estimated to be 88×10^{-6} ($k = 2$). In the final step $\mathcal{M}$ was used in conjunction with the density measurements from the first step to determine the compressibility factor, $Z = P\mathcal{M}/\rho R_u T$.

Following the GUM [xviii] the uncertainty in the measured compressibility factor

$$\left[\frac{u(Z_{meas})}{Z_{meas}}\right]^2 = \left[\frac{u(\mathcal{M})}{\mathcal{M}}\right]^2 + \left[\frac{u(P)}{P}\right]^2 + \left[\frac{u(T)}{T}\right]^2 + \left[\frac{u(\rho)}{\rho}\right]^2 + \left[\frac{u(R_u)}{R_u}\right]^2 \qquad \text{(B3)}$$

included standard uncertainty contributions (*i.e.*, $k = 1$) from the molar mass (44×10^{-6}); temperature (7×10^{-6}), pressure (31×10^{-6}), density (15×10^{-6}), and the universal gas constant (2×10^{-6}). Adding these components in quadrature and taking the square root gave a standard uncertainty of $\left[u(Z_{meas})/Z_{meas}\right] = 56 \times 10^{-6}$ ($k = 1$). The uncertainty of Z_{R8} (*i.e.*, the compressibility factor predicted by the REFPROP 8 Thermodynamic Database) includes uncertainty contributions from (1) the measured value of the compressibility factor; (2) the difference between the measured and predicted values of the compressibility factor at the same P, T, and x_k conditions; and (3) the gas composition values (x_k) determined by the GC relative to their actual values. An expression for the uncertainty of Z_{R8} that accounts for these three uncertainty sources is

$$\left[\frac{u(Z_{R8})}{Z_{R8}}\right]^2 = \left[\frac{u(Z_{meas})}{Z_{meas}}\right]^2 + \left|\frac{Z_{R8}/Z_{meas} - 1}{\sqrt{3}}\right|^2 + \sum_{k=1}^{K}\left(\frac{x_k}{Z}\frac{\partial Z}{\partial x_k}\right)^2\left(\frac{u(x_k)}{x_k}\right)^2 \qquad \text{(B4)}$$

where the difference between the measured and predicted Z values (*i.e.*, the second term) is assumed to follow a rectangular distribution so that its standard uncertainty was 219×10^{-6} for $k = 1$. to The last term accounts for the uncertainty in Z_{R8} caused by the uncertainty in mole fractions (x_k) measured by the gas chromatograph (GC). Monte Carlo simulations [xvii] predicted this uncertainty to be 80×10^{-6} ($k = 1$). In the simulation both the pressure and temperature are held fixed at 8018 kPa and 298.15 K, respectively, while each component in the composition was randomly varied in a Gaussian distribution centered around the measured gas composition. The uncertainty in the gas composition $u(x_k)$ included contributions from the uncertainty of the certified gas standard that was used to calibrate the GC, and the historical reproducibility of the GC. Based on Eqn. B4 the uncertainty of the $\left[u(Z_{R8})/Z_{R8}\right] = 240 \times 10^{-6}$ ($k = 1$).

As an additional check of the estimated uncertainty we compared the compressibility factor calculated by the REFPROP 8 Thermodynamic Database with values computed by three other databases including the AGA 8 [xxiv], GERG [xxv], and REFPROP 7 [xxvi] thermodynamic databases. Comparisons were made at the same pressure, temperature, and gas composition as used in the above analysis. The standard deviation of the four different thermodynamic databases

was 0.01 %. The good agreement of the four different equations of state gives a good indication that the gas mixture was well characterized at the conditions of interest. This result is not totally unexpected since the Iowa gas contains very little higher hydrocarbons as shown in Table 2.1 of Section 2.1.

Total Uncertainty of Species Molar Masses: $u_{tot}(M_k)$

The total uncertainty of the species molar masses is

$$u_{tot}^2(M_k) = \frac{1}{4}\sum_{k=1}^{K}\left(\frac{x_k M_k}{\mathcal{M}_{NG}}\right)^2\left[\frac{u(M_k)}{M_k}\right]^2 \tag{B5}$$

where M_k is the molar mass of the kth species, and $\mathcal{M}_{NG}$ is the molar mass of the natural gas, and the uncertainty of the molar mass of each component was estimated to be $[u(M_k)/M_k] = 10\times 10^{-6}$. Based on Eqn. B5 the total uncertainty of the species molar masses was $u_{tot}(M_k) = 4.5\times 10^{-6}$.

Total Gas Composition Uncertainty: $u_{tot}(x_k)$

The gas composition is measured using an industrial grade GC located upstream of the TMWS in the Iowa facility. The typical composition of gas at the Iowa facility is given in Table 2.1 of Section 2.1. Although the gas composition does not explicitly appear in Eqn. 4.12 used to determine the *K*-factor, it is contained in several of the variables. The three most significant variables influenced by x_k include the molar mass ($\mathcal{M}_{NG}$), the compressibility factor (Z_{TMWS}), and the critical flow function ($C_{s,NG}$). The composition is also needed to determine the Reynolds number of the HP CFVs (Re_{HP}) in Eqn 3.3, and the stagnation pressure (P_0) and temperature (T_0) given in Eqns. A1 and A2 of Appendix A. However, the uncertainty from these sources is small relative to the other components and are therefore omitted. Considering only contributions from the molar mass, the compressibility factor, and the critical flow function, the total uncertainty in gas composition is

$$u_{tot}^2(x_k) = \sum_{k=1}^{K}\left[\frac{1}{2}\left(\frac{x_k M_k}{\mathcal{M}_{NG}}\right) - \left(\frac{x_k}{C_s}\frac{\partial C_s}{\partial x_k}\right) - \left(\frac{x_k}{Z_{TMWS}}\frac{\partial Z_{TMWS}}{\partial x_k}\right)\right]^2\left[\frac{u(x_k)}{x_k}\right]^2 \tag{B6}$$

where $u(x_k)$ is the standard composition uncertainty. The linear sum of the sensitivity coefficients in Eqn. B6 accounts for correlated effects between $\mathcal{M}_{NG}$, Z_{TMWS}, and $C_{s,NG}$. A Monte Carlo simulation calculated the total composition uncertainty to be $u_{tot}(x_k) = 150 \times 10^{-6}$ ($k = 1$). The calculated uncertainty was significantly reduced by correlated effects between $\mathcal{M}_{NG}$, Z_{TMWS}, and $C_{s,NG}$ since separate Monte Carlo analysis on each of these variables indicated their individual uncertainties attributed to $u(x_k)$ to be $[u(\mathcal{M}_{NG})/\mathcal{M}_{NG}] = 300 \times 10^{-6}$, $[u(Z_{NG})/Z_{NG}] = 100 \times 10^{-6}$, and $[u(C_{s,NG})/C_{s,NG}] = 40 \times 10^{-6}$, respectively. All of the Monte Carlo calculations were done at constant pressure and temperature conditions of 298. 15 K and 7500 kPa, respectively.

APPENDIX B: Analysis of Selected Stage 4 Uncertainty Components

In the above analysis the uncertainty of the gas composition $u(x_k)$ was calculated as the root-sum-square of the uncertainty of the certified gas standard used to calibrate the GC, and the historical reproducibility of the GC. As a secondary estimate of $u(x_k)$, NIST collected gas samples from the Iowa facility and analyzed the composition independently by two different methods.

The first method collected a gas sample and had its composition measured by the Gas Metrology and Classical Methods Group at NIST. The difference in the molar mass of the two measurements was less than 0.05 %. The second method measured the molar mass using a two sinker densimeter (see the uncertainty of the compressibility factor above). The agreement between the molar mass computed from the Iowa GC composition measurements and the densimeter measurement was 0.023 %. Moreover, the molar mass measurement done using the densimeter was independent of gas composition. Therefore, the good agreement between the two measurements gives us confidence that the Iowa GC is performing adequately, and perhaps just as important is not omitting the measurement of any important constituents.

APPENDIX C: Analysis of Selected Stage 5 Uncertainty Components

Appendix C supports the uncertainty analysis of a MUT in Section 4.5. The calibration setup is shown in Fig. 2.1 of Section 2.2. A MUT is calibrated against a parallel array of up to nine TMWS. The TMWS are used to determine the volumetric flow at the MUT based either on Eqn. 2.8 of Section 2.3 or an analogous formulation given in Eqn. 4.15 of Section 4.5. The latter is more appropriate to use when using the GUM procedure [xviii] to determine uncertainty. Based on this procedure the uncertainty of volumetric flow is governed by Eqn. 4.16, and the values of components given in this equation are listed in Table 4.9. This appendix explains how numerical values were obtained for the following five uncertainty components: (1) $u_{\mathrm{tot}}(P)$, the total pressure uncertainty; (2) $u_{\mathrm{tot}}(T)$, the total temperature uncertainty; (3) $u_{\mathrm{tot}}(M_{\mathrm{k}})$, the total uncertainty of the species molar masses; (4) $u_{\mathrm{tot}}(Z)$, the total uncertainty of the compressibility factor; and (5) $u_{\mathrm{tot}}(x_{\mathrm{k}})$ the total uncertainty attributed to the measured gas composition.

Table C1. Uncertainty of pressure transducers used to measure the average pressure at the array of MUT

Unc. of Pressure at MUT	**Abs. Unc.**	**Rel. Std. Unc. (*k*=1)**	**Perc. Contrib.**	**Unc. Type**	**Comments**
MUT Pressure, P_{MUT} = 7173.9 kPa	(Pa)	(× 10^{-6})	(%)	A or B	
Uncorrelated Uncertainty					
Short Term Random Uncertainty[1]	1147.8	160	56.1	A	Calibration Control Charts
Long Term Random Uncertainty[1]	717.4	100	21.9	A	Calibration Control Charts
Data Acquisition (Agilent 34970A)	219.2	30.6	2.1	B	Manuf. spec.
Correlated Uncertainty					
Calibration Transfer Standard	414.2	57.7	7.3	A, B	Based on Manufactures Calib.
Ambient Temperature Effect	543.8	75.8	12.6	B	Manuf. spec.
Transducer mounting orientation	0	0	0	B	Always in same mounting position
Propagation of Uncorrelated Sources	***1371.2***	***191.1***	***80.1***		
Propagation of Correlated Sources	***683.6***	***95.3***	***19.9***		
Combined Uncertainty	**1532**	**214**	**100**		

Total Pressure Uncertainty: $u_{\mathrm{tot}}(P)$

During a flow calibration pressure measurements are made both at the MUT and at each of the TMWS being used. The uncertainty components for pressure measurements at the MUT are listed in Table C1. Although the uncertainty components for the TMWS pressure measurements are not shown, they are analogous to those shown in Table C1 for the MUT. The components are congruent since the nominal pressure being measured, the transducer type, and the standard used to calibrate both the MUT and the TMWS pressure transducers are the same.

[1] Short term random effects account for those effects that vary randomly during the time it takes to complete a single calibration while long term random effects include random variations between multiple calibrations.

APPENDIX C: Analysis of Selected Stage 5 Uncertainty Components

The total uncertainty of the pressure measurements includes uncertainty sources from both the TMWS and the MUT. Because all of the characterizations of these transducers are traceable to the same calibration standard, the bias uncertainty components are assumed to completely cancel and the total uncertainty in pressure is given by

$$u_{\text{tot}}^2(P) = \left[1 - \left(\frac{P}{Z}\frac{\partial Z}{\partial P}\right)\right]^2 \left(\left[\frac{u_{\text{u}}(P)}{P}\right]_{\text{MUT}}^2 + \frac{1}{N_5}\left[\frac{u_{\text{u}}(P)}{P}\right]_{\text{TMWS}}^2 \right) \qquad \text{(C1)}$$

where N_5 is the number of TMWS in use, the uncorrelated pressure components, $[u_{\text{u}}(P)/P]_{\text{MUT}}$ and $[u_{\text{u}}(P)/P]_{\text{TMWS}}$, both equal 191×10^{-6}. In addition, each transducer has the same random uncertainties. The random uncertainty components are from the short term random effects (160×10^{-6}), the long term random effects (100×10^{-6}), and the data acquisition (31×10^{-6}). When Eqn. (C1) is used with these values, the total pressure uncertainty equals $u_{\text{tot}}(P) = 263 \times 10^{-6}$.

Table C2. Uncertainty of temperature (T_{MUT}) at MUT

Unc. of HP CFV Temperature	**Abs. Unc.**	**Rel. Std. Unc. (*k*=1)**	**Perc. Contrib.**	**Unc. Type**	**Comments**
HP CFV Stag. Temp., T_{MUT}=295 K	(mK)	($\times 10^{-6}$)	(%)	A or B	
Uncorrelated Unc.					
Digital Accuracy	59	200	37.9	A	Manuf. Specs.
Stability	58.4	198	37.2		Manuf. Specs.
Data Acquisition (Agilent 34980A)	16.3	55	2.9	B	Manuf. spec. (Rect. Dist.)
RTD Self Heating	14.7	50	2.3	B	Exp. varied current
Correlated Unc.					
Temperature Transfer Standard	20	68	4.4	A, B	Manuf. Calibration
Ambient Temperature Effect	37.5	127	15.3	B	Manuf. spec. (Rect. Dist.)
Propagation of Uncorrelated Sources	***85.9***	***291***	***80.3***		
Propagation of Correlated Sources	***42.5***	***144***	***19.7***		
Combined Uncertainty	**95.8**	**325**	**100**		

Total Temperature Uncertainty: $u_{\text{tot}}(T)$

The temperatures at the MUT and at each of the TMWS are measured using a pair of the Rosemount 3144 RTDs. The uncertainty components for temperature measurements at the MUT are listed in Table C2. The analogous temperature components at the TMWS are not listed, but are similar in magnitude since the same transducer types are used, these transducers have been calibrated by the same temperature standard, and the transducers are used in application to measure the same nominal temperature.

APPENDIX C: Analysis of Selected Stage 5 Uncertainty Components

The total temperature uncertainty includes contributions from both the MUT and the TMWS. Because of the high degree of similarity between the TMWS and the MUT temperature measurements, bias uncertainty components completely cancel and the total relative uncertainty in temperature is given by

$$u_{\mathrm{tot}}^2(T) = \left[1 + \left(\frac{T}{Z}\frac{\partial Z}{\partial T}\right)\right]^2 \left(\left[\frac{u_{\mathrm{u}}(T)}{T}\right]_{\mathrm{MUT}}^2 + \frac{1}{N_5}\left[\frac{u_{\mathrm{u}}(T)}{T}\right]_{\mathrm{TMWS}}^2 \right) \tag{C2}$$

where N_5 is the number of TMWS in use, and the uncorrelated temperature uncertainty components, $\left[u_{\mathrm{u}}(T)/T\right]_{\mathrm{MUT}}$ and $\left[u_{\mathrm{u}}(T)/T\right]_{\mathrm{TMWS}}$, both equal 313×10^{-6}. In this case, the uncorrelated uncertainty components are assumed to include the digital accuracy (200×10^{-6}), the stability (198×10^{-6}), the ambient temperature effect (127×10^{-6}), the data acquisition (6×10^{-6}), and probe heat transfer effects (50×10^{-6}). Using these values in conjunction with Eqn. (C2), the total temperature uncertainty equals $u_{\mathrm{tot}}(T) = 340 \times 10^{-6}$.

Total Uncertainty of Species Molar Masses: $u_{\mathrm{tot}}(M_{\mathrm{k}})$

The total uncertainty of the species molar masses is

$$u_{\mathrm{tot}}^2(M_{\mathrm{k}}) = \left(1 - \frac{\mathcal{M}_{\mathrm{TMWS}}}{\mathcal{M}_{\mathrm{MUT}}}\right)^2 \sum_{\mathrm{k}=1}^{K} \left(\frac{x_{\mathrm{k}} M_{\mathrm{k}}}{\mathcal{M}_{\mathrm{MUT}}}\right)^2 \left[\frac{u(M_{\mathrm{k}})}{M_{\mathrm{k}}}\right]^2 . \tag{C3}$$

where $\mathcal{M}_{\mathrm{MUT}}$ and $\mathcal{M}_{\mathrm{TMWS}}$ are the molar masses at the TMWS and MUT, respectively. Since these molar masses are practically equal (*i.e.*, $\mathcal{M}_{\mathrm{MUT}} = \mathcal{M}_{\mathrm{TMWS}}$ in Eqn. C3), $u_{\mathrm{tot}}(M_{\mathrm{k}})$ is identically zero.

Total Uncertainty of Gas Composition: $u_{\mathrm{tot}}(x_{\mathrm{k}})$

During a Stage 5 flowmeter calibration the gas composition (or mole fraction; x_{k}) will differ slightly between the MUT and the TMWS. This difference in x_{k} results from small fluctuations in the gas composition entering the Iowa flow facility. Since the residence times differ for the gas to travel from the measurement location to the MUT versus the TMWS, the instantaneous values of composition differ at these two locations. The resulting uncertainty attributed to this difference is

$$u_{\mathrm{tot}}^2(x_{\mathrm{k}}) = \sum_{\mathrm{k}=1}^{K} \left(\frac{x_{\mathrm{k}}}{Z}\frac{\partial Z}{\partial x_{\mathrm{k}}} - \frac{x_{\mathrm{k}}}{\mathcal{M}}\frac{\partial \mathcal{M}}{\partial x_{\mathrm{k}}} \right)^2 \left[\frac{\sigma_{x_{\mathrm{k}}}}{x_{\mathrm{k}}}\right]^2 \tag{B3}$$

where σ_{x_k}/x_k is the standard deviation of typical fluctuations for each species in the natural gas mixture. This uncertainty is conservatively estimated to be large, including, the reproducibility of the gas chromatograph used to make the composition measurements. Using this expression the total uncertainty in gas composition is $u_{\mathrm{tot}}(x_{\mathrm{k}}) = 208 \times 10^{-6}$.

Total Uncertainty of the Compressibility Factor: $u_{\mathrm{tot}}(Z)$

The compressibility factor is determined at the MUT as well as at each TMWS being used. In all cases, the REFPROP 8.0 Thermodynamic Database [ii] is used to evaluate the compressibility

factor. Since the nominal pressure, temperature, and gas composition are the same at the MUT and at the TMWS array, the uncertainty resulting from the thermodynamic database completely cancels, yielding a zero uncertainty.

National Institute of Standards and Technology
Technology Administration, U.S. Department of Commerce

APPENDIX D:
SAMPLE CALIBRATION REPORT

FOR

AN ULTRASONIC FLOWMETER

July 8, 2007

Mfg.: Ultrasonic Flowmeter Builders, Inc.
Serial Number: 1234
Bore Diameter: 30.322 cm (11.938 inch)

submitted by

Advanced Technology Ultrasonics, Inc.
1829 Flowmeter Rd.
Metertown, MD 123456

Purchase Order No. A123 dated June 24, 2007

The ultrasonic flowmeter identified above was calibrated in dry pipeline quality natural gas using a parallel array of three turbine meter working standards. The calibration was completed in accordance with the American Gas Association Transmission Report Number 9 [5]. Thermodynamic properties (*e.g.*, speed of sound, density, etc.) are computed using the REFPROP 8.0 Thermodynamic Database [6] in its AGA 8 mode. This database is effectively equivalent to the AGA 10 Thermodynamic database, having sound speed and density values that agree with the AGA 10 model to better than 0.00001% and 0.000002 %, respectively over the range of pressures, temperatures, and gas compositions relevant to this calibration. The calibration was performed at the Colorado Engineering Experimental Station Incorporated (CEESI) flow facility located at 2365 240th St. in Garner, Iowa 50438 under NIST's metrological control. The traceability of all auxiliary flow measurements for pressure, temperature, frequency, etc. are maintained by NIST. In addition, flow determination is based on an array of the turbine

[5] American Gas Association (AGA); *Measurement of Gas by Multipath Ultrasonic Meters*; Transmission Measurement Committee Report No. 9 2nd edition (AGA9), AGA, April 2007.

[6] Lemmon, E. W., et. al., *REFPROP 23: Reference Fluid Thermodynamic and Transport Properties, NIST Standard Reference Database 23, Version 8*, National Institute of Standards and Technology, Boulder, Colorado, 2007.

meter working standards that are traceable to NIST's primary flow standards via a bootstrap process using critical flow venturis transfer standards.[7,8]

The flowmeter was calibrated at six flows and at each flow, three (or more) measurements were gathered on two different occasions. These measurements are used to produce averages at each of the six flows so that the plots are averages of six or more individual calibration measurements. This report contains tabulations of both the averaged flow results and the individual data points. At the conclusion of the calibration, the flow adjustment is electronically installed in the flowmeter and single verification point is taken to confirm proper meter operation.

The ultrasonic flowmeter of bore diameter of $D =$ 30.322 cm (11.938 inch) and serial number 1234 was installed in a piping test section of approximately 30.48 cm (12 inch) diameter located downstream of the turbine meter array. The volumetric flow (Q_{NIST}) at the meter under test was determined by summing the flow through all of the open turbine meter working standards and applying conservation of mass. A photograph of the flowmeter installation is shown in Figure 1. Table 1 shows the pressure, temperature, and data acquisition system used in the calibration. The nominal temperature and pressure during the test was 295.44 K (72.12 °F) and 8 376.9 kPa (1 215.0 psia), respectively. The serial numbers of the three turbine meter working standards used to determine the volumetric flow are 97500360 (1), 95380241 (2), and 7500361 (3), respectively, where the number in parenthesis immediately following the serial number specifies the position of the turbine meter in the array at the time of calibration. The nominal composition of the natural gas mixture during the calibration and verification is given in Table 3.

Figure 1. Photograph of the flowmeter installed in the pipeline

[7] Johnson, A. N. and Wright, J. D., *Gas Flowmeter Calibrations with the 26 m³ PVTt Standard*, NIST Special Publication 250-1046, National Institute of Standards and Technology, Gaithersburg, MD, (2006).

[8] Johnson, A. N. and Kegel, T. *Uncertainty and Traceability for the CEESI Iowa Natural Gas Facility*, J. Res. Natl. Inst. Stand. Technol., 109, pp. 345-369 (2004).

Table 1. Specification of data acquisition system, the pressure transducers, and the temperature transducers used for the calibration.

Data Acquisition	Barometric Pressure	Gauge Pressure	Temperature
Agilent 34980 A (QC #999)	PCU 300 (QC # 300)	2 Rosemount 3051 Pressure Transmitters (QC# 901 & 902)	2 Rosemount 3144 RTD Transmitters (QC# 950 & 951)

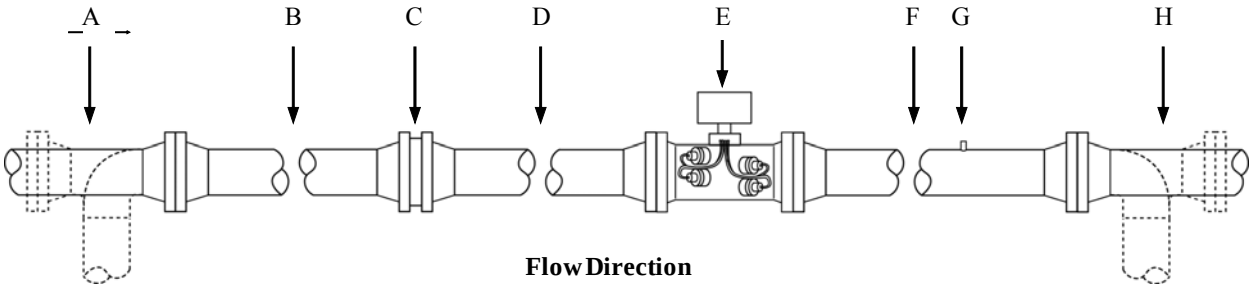

Figure 2. Labeling of uni-directional flowmeter installation configuration (Labels are described in Table 2) This piping configuration meets straight-run requirements for AGA9**.**

Table 2. Itemized list detailing the piping sections (*e.g.*, lengths, orientation, serial numbers); the flowmeter being calibrated (*e.g.*, type, size, serial number); the flow conditioner (*e.g.*, type, orientation, serial number); and thermowell location during the calibration process in Fig. 2

Components Specified in Fig. 2	Description
A – Pipe Section (Straight pipe or Elbow)	Straight Pipe.
B – Pipe Section	Length = 5.1 *D* , (SN 01-111345)
C – Flow Conditioner	Flow Profile Fixer (SN -02-12345); Flow direction and mounting location verified
D – Pipe Section	Length = 5.03 *D* , (SN 01-111346)
E – Flowmeter	Ultrasonic Flowmeter Builders with diameter (SN 1234)
F – Pipe Section	Length = 5.05 *D* , (SN 01-111347)
G – Thermowell Location	Distance to closest flowmeter flange face is 2 *D*
H – Pipe Section (Straight pipe or Elbow)	Straight Pipe.

Table 3. Normalized gas composition measured with gas chromatograph (SN 9007671) at the start and end of the calibration, and at the start and end of the verification point.

Component	Normalized Mole Fraction (%)			
	Start of Calibration	End of Calibration	Start of Verification Point	End of Verification Point
Methane	94.8865	94.9474	94.9355	94.937
Ethane	2.3172	2.2630	2.2709	2.2712
Propane	0.2264	0.2176	0.2170	0.2177
Iso Butane	0.0185	0.0181	0.0179	0.0181
Butane	0.0228	0.0222	0.0218	0.0223
Iso Pentane	0.0050	0.0051	0.0052	0.0049
Pentane	0.0037	0.0037	0.0037	0.0038
Hexane (C6+)	0.005	0.005	0.0049	0.0049
Nitrogen	1.6206	1.6422	1.6479	1.6457
Carbon Dioxide	0.6543	0.6330	0.638	0.6392
Hydrogen	0.2053	0.2080	0.2019	0.2006
Helium	0.0347	0.0347	0.0353	0.0346
Heating Value	1 012.1	1 011.5	1 003.6	1 003.6
Total Un-Normalized	99.9012	99.9012	99.9012	99.9012

The velocity in the piping immediately upstream of the ultrasonic flow meter is determined by dividing the NIST's volumetric flow (Q_{NIST}) determined by the turbine meter working standards by the piping cross sectional area ($A_{\text{cs}} = \pi D^2/4$)

$$V_{\text{NIST}} = \frac{Q_{\text{NIST}}}{A_{\text{cs}}} = \frac{4Q_{\text{NIST}}}{\pi D^2} \tag{1}$$

where D = 30.322 cm (11.938 inch). The calibration factor is

$$\phi = \frac{V_{\text{NIST}}}{V_{\text{meter}}} = \frac{Q_{\text{NIST}}}{Q_{\text{meter}}} \tag{2}$$

the ratio of the NIST measured velocity (V_{NIST}) and the velocity reported by the flowmeter (V_{meter}), or alternatively, the ratio of the NIST's determined volumetric flow (Q_{NIST}) divided by the meter volumetric flow ($Q_{\text{meter}} = \pi D^2 V_{\text{meter}}/4$). The calibration factor is defined so that when it is multiplied with the meter velocity (or the meter volumetric flow) the result is the NIST calibrated velocity (or NIST volumetric flow). The error in the meter volumetric flow is defined as the percent difference between the NIST value and the meter reported value

$$\varepsilon = 100\left(\frac{Q_{\text{meter}}}{Q_{\text{NIST}}} - 1\right) = 100\left(\frac{1-\phi}{\phi}\right). \quad (3)$$

which can also be expressed in terms of the calibration factor.

The calibration results are presented in Figure 3 and in Table 4. Figure 3 plots the velocity determined by the Turbine meter standards versus the error and Table 4 gives the averaged calibration results and their expanded uncertainty. In addition, the speed of sound calculated by the flowmeter is compared to values computed the REFPROP 8.0 Thermodynamic Database at the measured pressure, temperature, and gas composition. Table 5 shows the individual data points (*i.e.*, before averaging) for the calibration process.

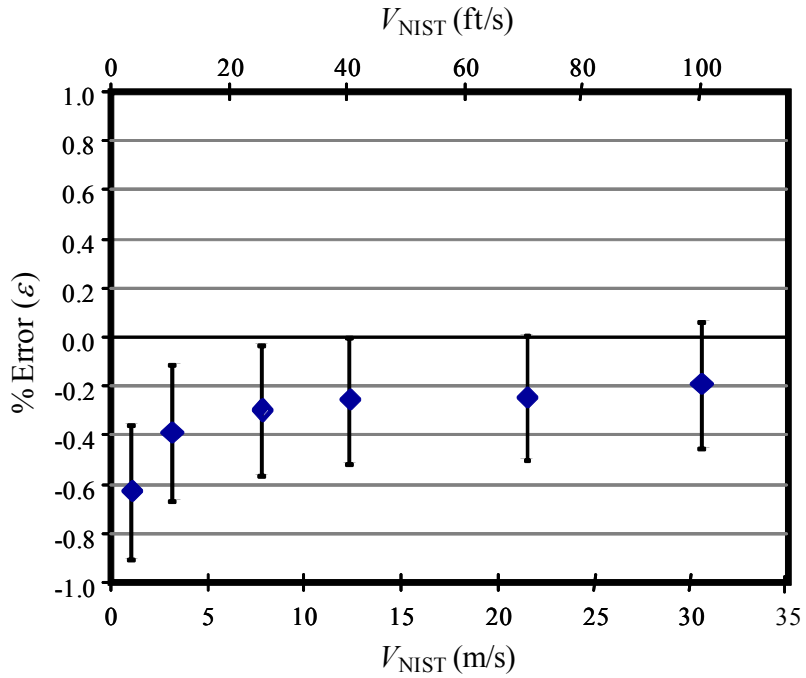

Figure 3. Calibration results showing the percent difference in NIST flow (Q_{NIST}) with the measured flow (Q_{meter}) plotted versus the reported meter velocity (V_{NIST}) for ultrasonic flowmeter serial number 1234. The error bars denote the combined expanded uncertainties shown in Table 4. (For convenience the velocity units are plotted both in m/s and ft/s.)

Table 4. Calibration results for ultrasonic flowmeter serial number 1234. (The results are tabulated in both SI and English units.)

Flow [% FS]	**NIST Velocity** (V_{NIST}) [m/s]	**Meter Flow** (Q_{meter}) [m^3/s]	**NIST Flow** (Q_{NIST}) [m^3/s]	**% Flow Error** (ε) [%]	**Calib. Factor** (ϕ) [ ]	**Expand. Unc.** (U_e) [%]	**REFPROP 8.0 Sound Speed** [m/s]	**Meter Avg Sound Speed** [m/s]	**% Diff. Sound Speed** [%]
100	30.724	2.2143	2.2186	-0.20	1.0020	0.26	423.31	423.31	0.00
70	21.508	1.5492	1.5531	-0.25	1.0025	0.26	423.79	423.71	0.02
40	12.291	0.8853	0.8876	-0.26	1.0026	0.26	424.04	424.02	0.00
25	7.6828	0.5531	0.55478	-0.30	1.0031	0.27	424.08	423.98	0.02
10	3.0742	0.22112	0.22199	-0.40	1.0039	0.28	423.84	423.75	0.02
3	0.9151	0.06566	0.06608	-0.64	1.0064	0.28	423.63	423.47	0.04
[% FS]	[ft/s]	[acfh]	[acfh]	[%]	[ ]	[%]	[ft/s]	[ft/s]	[%]
100	100.80	281 506	282 061	-0.20	1.0020	0.26	1 388.82	1 388.80	0.002
70	70.56	196 954	197 448	-0.25	1.0025	0.26	1 390.40	1 390.11	0.02
40	40.326	112 546	112 839	-0.26	1.0026	0.26	1 391.20	1 391.15	0.00
25	25.206	70 317	70 531	-0.30	1.0031	0.27	1 391.35	1 391.01	0.02
10	10.086	28 111.0	28 222.0	-0.40	1.0039	0.28	1 390.54	1 390.27	0.02
3	3.002	8 347.3	8 401.7	-0.64	1.0064	0.28	1 389.85	1 389.34	0.04

Table 5. Calibration results of point by point data for ultrasonic flowmeter serial number 1234.

Pt	Time	NIST Velocity (V_{NIST})	Meter Flow (Q_{meter})	NIST Flow (Q_{NIST})	% Flow. Error (ε)	Calib. Factor (ϕ)	Temp.	Pres.	REFPROP 8.0 Sound Speed	Avg. Meter Sound Speed	% Sound Speed Diff.
[ ]	[ ]	[m/s]	[m^3/s]	[m^3/s]	[%]	[ ]	[K]	[kPa]	[m/s]	[m/s]	[%]
1	7:01:25 AM	30.722	2.2138	2.2185	-0.21	1.0021	295.21	8 313.0	423.27	423.24	0.006
2	7:03:40 AM	30.725	2.2141	2.2187	-0.21	1.0021	295.24	8 307.6	423.32	423.31	0.003
3	7:05:47 AM	30.726	2.2146	2.2188	-0.19	1.0019	295.27	8 306.3	423.35	423.37	-0.007
4	7:11:30 AM	21.504	1.5492	1.5528	-0.23	1.0023	295.57	8 349.8	423.78	423.69	0.021
5	7:13:47 AM	21.509	1.5491	1.5532	-0.26	1.0026	295.58	8 350.1	423.78	423.70	0.019
6	7:15:48 AM	21.504	1.5489	1.5528	-0.25	1.0025	295.58	8 350.2	423.82	423.73	0.023
7	7:21:04 AM	12.292	0.8852	0.8876	-0.27	1.0027	295.65	8 390.2	424.03	424.00	0.006
8	7:23:07 AM	12.289	0.8852	0.8874	-0.25	1.0025	295.66	8 388.9	424.03	424.02	0.002
9	7:25:27 AM	12.289	0.885	0.8874	-0.27	1.0027	295.67	8 388.9	424.05	424.05	0.000
10	7:30:56 AM	7.6844	0.553	0.5549	-0.34	1.0034	295.69	8 401.5	424.14	424.05	0.021
11	7:33:19 AM	7.6761	0.5526	0.5543	-0.31	1.0031	295.63	8 401.3	424.08	423.98	0.024
12	7:35:40 AM	7.6913	0.5536	0.5554	-0.32	1.0033	295.58	8 400.8	424.03	423.91	0.027
13	7:41:24 AM	3.0695	0.2207	0.22165	-0.43	1.0043	295.49	8 407.6	423.92	423.83	0.022
14	7:43:28 AM	3.0663	0.22055	0.22142	-0.39	1.0039	295.42	8 405.8	423.84	423.75	0.022
15	7:45:35 AM	3.0796	0.2216	0.22238	-0.35	1.0035	295.34	8 404.4	423.75	423.68	0.017
16	7:51:25 AM	0.9147	0.06566	0.06605	-0.59	1.0059	295.21	8 407.7	423.70	423.56	0.034
17	7:53:48 AM	0.9217	0.06613	0.06656	-0.65	1.0065	295.12	8 406.0	423.62	423.45	0.041
18	7:56:09 AM	0.9155	0.06568	0.06611	-0.65	1.0065	295.06	8 404.5	423.56	423.40	0.038
Shutdown Flow and Reestablish Set point											
19	8:12:49 AM	0.9141	0.06563	0.06601	-0.58	1.0058	295.06	1 219.0	423.56	423.40	0.038
20	8:14:50 AM	0.9126	0.06544	0.0659	-0.70	1.0070	295.12	1 219.2	423.62	423.45	0.041
21	8:17:01 AM	0.9118	0.06541	0.06584	-0.65	1.0066	295.21	1 219.4	423.70	423.56	0.034
22	8:22:10 AM	3.0735	0.2211	0.22194	-0.38	1.0038	295.34	1 219.0	423.75	423.68	0.017
23	8:24:12 AM	3.0768	0.22136	0.22218	-0.37	1.0037	295.42	1 219.2	423.84	423.75	0.022
24	8:26:19 AM	3.0793	0.22138	0.22236	-0.44	1.0044	295.49	1 219.4	423.92	423.83	0.022
25	8:31:48 AM	7.6761	0.5527	0.5543	-0.29	1.0029	295.58	1 218.4	424.03	423.91	0.027
26	8:34:05 AM	7.6899	0.5539	0.5553	-0.25	1.0025	295.63	1 218.5	424.08	423.98	0.024
27	8:36:08 AM	7.6788	0.5528	0.5545	-0.31	1.0031	295.69	1 218.5	424.14	424.05	0.021
28	8:41:47 AM	12.289	0.8851	0.8874	-0.26	1.0026	295.67	1 216.7	424.05	424.05	0.000
29	8:43:58 AM	12.296	0.8857	0.8879	-0.25	1.0025	295.66	1 216.7	424.03	424.02	0.002
30	8:46:00 AM	12.293	0.8854	0.8877	-0.26	1.0026	295.65	1 216.9	424.03	424.00	0.006
31	8:51:30 AM	21.510	1.5493	1.5533	-0.26	1.0026	295.58	1 211.1	423.82	423.73	0.023
32	8:53:32 AM	21.508	1.5495	1.5531	-0.23	1.0023	295.58	1 211.1	423.78	423.70	0.019
33	8:55:53 AM	21.510	1.5492	1.5533	-0.26	1.0026	295.57	1 211.0	423.78	423.69	0.021
34	9:01:34 AM	30.721	2.2142	2.2184	-0.19	1.0019	295.27	1 204.7	423.35	423.37	-0.007
35	9:03:53 AM	30.726	2.2144	2.2188	-0.20	1.0020	295.24	1 204.9	423.32	423.31	0.003
36	9:05:58 AM	30.724	2.2145	2.2186	-0.19	1.0019	295.21	1 205.7	423.27	423.24	0.006

Upon Completion of the calibration the coefficients in Table 6 listed below were input into the meter and then the meter was put into a *Read Only* mode. Subsequently a single verification point was done as shown in Figure 5 and in Tables 7 and 8, respectively.

Table 6. Calibration coefficients electronically installed in ultrasonic flowmeter serial number 1234.

Register	Name	Value	Register	Name	Value
328	FwdFlwRt1	281 506	340	FwdMtrFctr1	1.0020
329	FwdFlwRt2	196 954	341	FwdMtrFctr2	1.0025
330	FwdFlwRt3	112 546	342	FwdMtrFctr3	1.0026
331	FwdFlwRt4	70 317	343	FwdMtrFctr4	1.0031
332	FwdFlwRt5	28 111.0	344	FwdMtrFctr5	1.0039
333	FwdFlwRt6	8 347.3	345	FwdMtrFctr6	1.0064
334	FwdFlwRt7	0	346	FwdMtrFctr7	1
335	FwdFlwRt8	0	347	FwdMtrFctr8	1
336	FwdFlwRt9	0	348	FwdMtrFctr9	1
337	FwdFlwRt10	0	349	FwdMtrFctr10	1
338	FwdFlwRt11	0	350	FwdMtrFctr11	1
339	FwdFlwRt12	0	351	FwdMtrFctr12	1

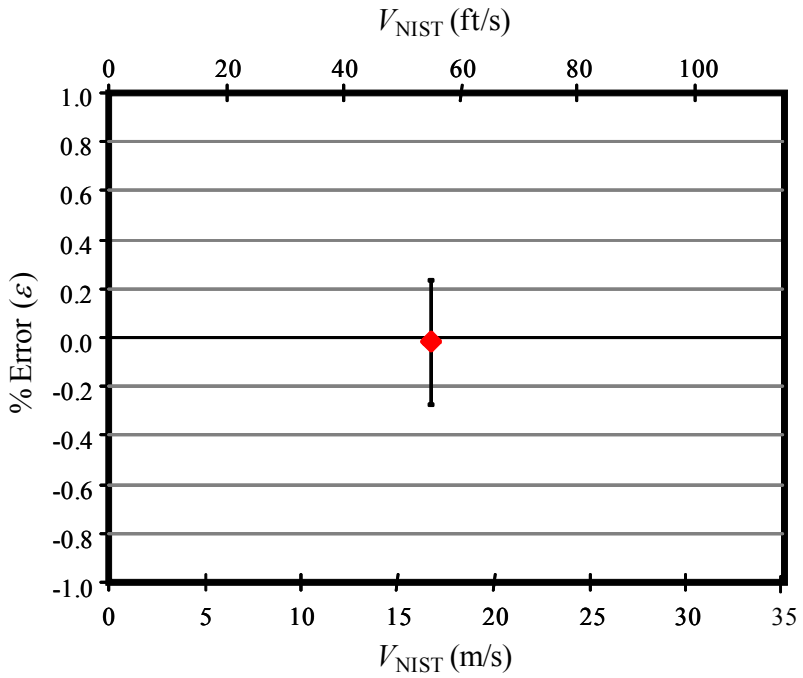

Figure 4. Verification results showing the error percent difference in NIST flow (Q_{NIST}) with the measured flow (Q_{meter}) plotted versus the reported meter velocity (V_{NIST}) for ultrasonic flowmeter serial number 1234. The error bar represents the combined expanded uncertainty shown in Table 7.

Table 7. Single point verification results for ultrasonic flowmeter serial number 1234. (The results are tabulated in both SI and English units.)

Flow [% FS]	**NIST. Velocity** (V_{NIST}) [m/s]	**Meter Flow** (Q_{meter}) [m^3/s]	**NIST Flow** (Q_{NIST}) [m^3/s]	**% Flow Error** (ε) [%]	**REFPROP 8.0 Sound Speed** [m/s]	**Meter Avg Sound Speed** [m/s]	**% Diff. Sound Speed** [%]
55	16.896	1.2200	1.2201	-0.01	423.93	423.92	0.002
[% FS]	[ft/s]	[acfh]	[acfh]	[%]	[ft/s]	[ft/s]	[%]
55	55.434	155 102	155 119	-0.01	1 390.85	1 390.81	0.002

Table 8. **Verification** results of point by point data for ultrasonic flowmeter serial number 1234.

Pt [ ]	Time [ ]	NIST Velocity (V_{NIST}) [m/s]	Meter Flow (Q_{meter}) [m^3/s]	NIST Flow (Q_{NIST}) [m^3/s]	% Flow. Error (ε) [%]	Temp. [K]	Pres. [kPa]	REFPROP 8.0 Sound Speed [m/s]	Avg. Meter Sound Speed [m/s]	% Sound Speed Diff. [%]
1	9:19:56 AM	16.893	1.2196	1.2199	-0.02	295.49	8 374.1	423.89	423.83	0.014
2	9:22:01 AM	16.893	1.2199	1.2199	0.00	295.57	8 373.3	423.94	423.93	0.002
3	9:24:14 AM	16.903	1.2205	1.2206	-0.01	295.59	8 371.1	423.96	423.99	-0.007

Updated register files produced by the flowmeter are also provided with each calibration report. These files are not included in this sample report since the content and format of these files differ substantially among flowmeter manufactures.

An analysis was performed to assess the uncertainty of the results obtained for the meter under test.[5,6,7] The process involves identifying the equations used in calculating the calibration result (measurand) so that the sensitivity of the result to uncertainties in the input quantities can be evaluated. The approximately 67 % confidence level uncertainty of each of the input quantities is determined, weighted by its sensitivity, and combined with the other uncertainty components by root-sum-square to arrive at a combined uncertainty (u_c). The combined uncertainty is multiplied by a coverage factor of $k = 2.0$ to arrive at an expanded uncertainty (U_e) of the measurand with approximately 95% confidence level.

As described in the references, if one considers a generic basis equation for the measurement process, which has an output, y, based on N input quantities, x_i,

$$y = y(x_1, x_2, \ldots, x_N) \tag{4}$$

and all uncertainty components are uncorrelated, the normalized expanded uncertainty is given by,

$$\frac{U_e(y)}{y} = k\frac{u_c(y)}{y} = k\sqrt{\sum_{i=1}^{N} s_i^2 \left(\frac{u(x_i)}{x_i}\right)^2} \tag{5}$$

In the normalized expanded uncertainty equation, the $u(x_i)'s$ are the standard uncertainties of each input, and $s_i's$ are their associated sensitivity coefficients, given by,

$$s_i = \frac{\partial y}{\partial x_i}\frac{x_i}{y} \tag{6}$$

The normalized expanded uncertainty equation is convenient since it permits the usage of relative uncertainties (in fractional or percentage forms) and of dimensionless sensitivity coefficients. The dimensionless sensitivity coefficients can often be obtained by inspection since for a linear function they have a magnitude of unity.

For this calibration, the uncertainty includes the base uncertainty as determined in the SP250 Supplement for natural gas flow measurements[3] and the reproducibility[8] of the measurements. The values of uncertainty given in Table 4 include contribution from both these sources. To

---

5 International Organization for Standardization, *Guide to the Expression of Uncertainty in Measurement*, Switzerland, 1996 edition.

6 Taylor, B.N. and Kuyatt, C.E., *Guidelines for Evaluating and Expressing the Uncertainty of NIST Measurement Results*, NIST TN 1297, 1994 edition.

7 Coleman, H.W. and Steele, W.G., *Experimentation and Uncertainty Analysis for Engineers*, John Wiley and Sons, 2nd ed., 1999.

8 Reproducibility is herein defined as the closeness of agreement between measurements with the flow changed and then returned to the same nominal value

measure the reproducibility of the test, the standard deviation of the discharge coefficient at each of the nominal flows was used to calculate the relative standard uncertainty (the standard deviation divided by the mean and expressed as a percentage). The reproducibility was propagated along with the other uncertainty components to calculate the combined uncertainty. Using the values given above, results in the expanded uncertainties listed in the data table and shown as error bars in Figure 4.

For the Director,
National Institute of Standards and Technology

Project Leader's Official Signature

Aaron Johnson
Fluid Metrology Group
Process Measurements Division
Chemical Science and Technology Laboratories